

1
2 **Standard multiscale entropy reflects spectral power at**
3 **mismatched temporal scales: What's signal irregularity**
4 **got to do with it?**
5

6
7 Short title: Multi-scale entropy reflects spectral power
8

9
10 Julian Q. Kosciessa^{123*}, Niels A. Kloosterman¹², and Douglas D. Garrett^{12*}
11

12 ¹Max Planck UCL Centre for Computational Psychiatry and Ageing Research, Berlin,
13 Germany

14 ²Center for Lifespan Psychology, Max Planck Institute for Human Development, Berlin,
15 Germany

16 ³Department of Psychology, Humboldt-Universität zu Berlin, Berlin, Germany
17

18 * Corresponding authors: kosciessa@mpib-berlin.mpg.de; garrett@mpib-berlin.mpg.de
19
20
21

22 **Author ORCIDs**

23 Julian Q. Kosciessa – <http://orcid.org/0000-0002-1134-7996>

24 Niels A. Kloosterman – <http://orcid.org/0000-0002-1134-7996>

25 Douglas D. Garrett – <https://orcid.org/0000-0002-0629-7672>
26
27

28 **Keywords**

29 multiscale sample entropy; irregularity; resting state EEG; age differences; rhythms

30 **Abstract**

31 Multiscale Entropy (MSE) is increasingly used to characterize the temporal irregularity
32 of neural time series patterns. Due to its' presumed sensitivity to non-linear signal
33 characteristics, MSE is typically considered a complementary measure of brain dynamics to
34 signal variance and spectral power. However, the divergence between these measures is often
35 unclear in application. Furthermore, it is commonly assumed (yet sparingly verified) that
36 entropy estimated at specific time scales reflects signal irregularity at those precise time scales
37 of brain function. We argue that such assumptions are not tenable. Using simulated and
38 empirical electroencephalogram (EEG) data from 47 younger and 52 older adults, we indicate
39 strong and previously underappreciated associations between MSE and spectral power, and
40 highlight how these links preclude traditional interpretations of MSE time scales. Specifically,
41 we show that the typical definition of temporal patterns via "similarity bounds" biases coarse
42 MSE scales – that are thought to reflect slow dynamics – by high-frequency power. Moreover,
43 we demonstrate that entropy at fine time scales – presumed to indicate fast dynamics – is highly
44 sensitive to broadband spectral power, a measure dominated by low-frequency contributions.
45 Jointly, these issues produce counterintuitive reflections of frequency-specific content on MSE
46 time scales. We emphasize the resulting inferential problems in a conceptual replication of
47 cross-sectional age differences at rest, in which scale-specific entropy age effects could be
48 explained by spectral power differences at mismatched temporal scales. Furthermore, we
49 demonstrate how such problems may be alleviated, resulting in the indication of scale-specific
50 age differences in rhythmic irregularity. Finally, we recommend best practices that may better
51 permit a valid estimation and interpretation of neural signal irregularity at time scales of
52 interest.

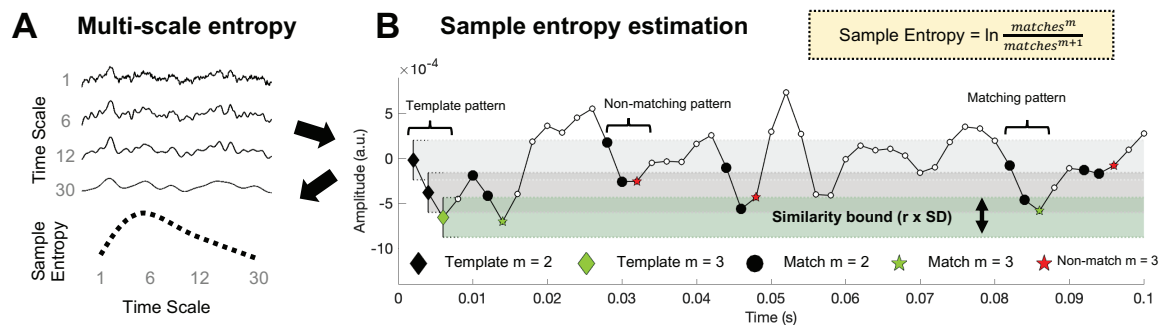
53 **Author Summary**

54 Brain signals exhibit a wealth of dynamic patterns that that are thought to reflect
55 ongoing neural computations. Multiscale sample entropy (MSE) intends to describe the
56 temporal irregularity of such patterns at multiple time scales of brain function. However, the
57 notion of time scales may often be unintuitive. In particular, traditional implementations of
58 MSE are sensitive to slow fluctuations at fine time scales, and fast dynamics at coarse time
59 scales. This conceptual divergence is often overlooked and may lead to difficulties in
60 establishing the unique contribution of MSE to effects of interest over more established spectral
61 power. Using simulations and empirical data, we highlight these issues and provide evidence
62 for their relevance for valid practical inferences. We further highlight that standard MSE and
63 traditional spectral power are highly collinear in our example. Finally, our analyses indicate
64 that spectral filtering can be used to estimate temporal signal irregularity at matching and
65 intuitive time scales. To guide future studies, we make multiple recommendations based on our
66 observations. We believe that following these suggestions may advance our understanding of
67 the unique contributions of neural signal irregularity to neural and cognitive function across the
68 lifespan.

69 Introduction

70 Entropy as a measure of signal irregularity

71 Neural time series exhibit a wealth of dynamic patterns that are thought to reflect
 72 ongoing neural computations. While some of these patterns consist of stereotypical deflections
 73 [e.g., periodic neural rhythms; 1, 2], the framework of nonlinear dynamics and complex systems
 74 increasingly emphasizes the importance of temporal irregularity (or variability) for healthy,
 75 efficient, and flexible neural function [3-6]. In parallel with such conceptual advances,
 76 multiscale entropy (MSE) [7, 8], an information-theoretic index that estimates sample entropy
 77 [9] at multiple time scales (Fig 1A), is increasingly applied to quantify the irregularity of neural
 78 time series across different brain states, the lifespan, and in relation to health and disease [10-
 79 18].
 80



81
 82 **Fig 1.** Traditional MSE estimation procedure. (A) Multi-scale entropy is an extension of sample entropy, an
 83 information-theoretic metric intended to describe the temporal irregularity of time series data. To estimate entropy
 84 for different time scales, the original signal is traditionally ‘coarse-grained’ using low-pass filters, followed by the
 85 calculation of the sample entropy. (B) Sample entropy estimation procedure. Sample entropy measures the
 86 conditional probability that two amplitude patterns of sequence length m (here, 2) remain similar (or matching)
 87 when the next sample $m + 1$ is included in the sequence. Hence, sample entropy increases with temporal
 88 irregularity, i.e., with the number of m -length patterns that do not remain similar at length $m+1$ (non-matches). To
 89 discretize temporal patterns from continuous amplitudes, similarity bounds (defined as a proportion r , here .5, of
 90 the signal variance) define amplitude ranges around each sample in a given template sequence, within which
 91 matching samples are identified in the rest of the time series. These are indicated by horizontal grey and green bars
 92 around the first three template samples. This procedure is applied to each template sequence in time, and the pattern
 93 counts are summed to estimate the signal’s entropy. The exemplary time series is a selected empirical EEG signal
 94 that was 40-Hz high-pass filtered with a 6th order Butterworth filter.

95
 96 In general, sample entropy quantifies the irregularity of temporal patterns in a given
 97 signal (for an example of its calculation, see Fig 1B). Whereas signals with a repetitive structure
 98 (like stationary signals or rhythmic fluctuations) are estimated as having low entropy, less
 99 predictable (or random) signals are ascribed high entropy. As an extension of this principle,
 100 MSE aims to describe temporal irregularity at different time scales – varying from fine (also
 101 referred to as ‘short’) to coarse (or ‘long’). In conventional Fourier analysis of time series data,
 102 time scales are quantified in terms of lower and higher frequencies present in the signal. This
 103 has been shown to be a principled time scale descriptor that relates at least in part to structural
 104 properties of the generating neural circuits [2, 19-22]. Given this meaningful definition of fast
 105 and slow events, it is a common assumption – including in guides to MSE’s interpretation in

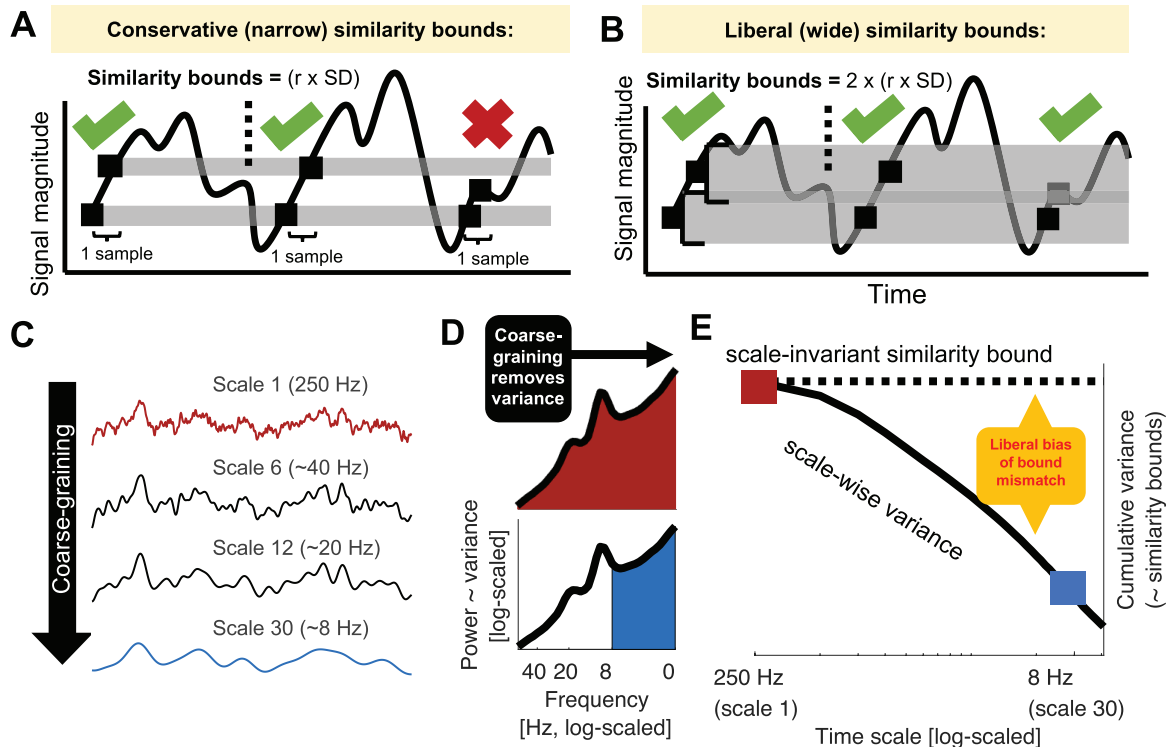
106 neural applications [23] – that fine-to-coarse scales characterize the irregularity of high-to-low
107 frequency dynamics, respectively. However, here we identify one methodological and one
108 conceptual issue regarding the computation of MSE that challenge such a direct scale-to-
109 frequency mapping. First, we first show that the traditional definition of temporal patterns may
110 lead to an influence of high frequencies on coarse entropy time scales (Issue 1). Second, we
111 establish that the signal content at fine time scales renders entropy estimates sensitive to slow
112 fluctuations (Issue 2).

113 Due to its assessment of temporal patterns rather than oscillatory dynamics, MSE has
114 been motivated as a complementary measure to spectral variance/power that is sensitive to non-
115 linear signal characteristics, such as phase shifts or cross-frequency coupling. [Note that we use
116 the terms power and variance interchangeably, as a time domain signal’s broadband variance is
117 proportional to the integral of its power spectral density, while narrowband variance in the time
118 domain is identical to narrowband power in the spectral domain.] However, the overlap between
119 these measures is often unclear in application because the mapping between spectral power and
120 scale-wise entropy is ambiguous. Such ambiguity affects both the ability to compare individuals
121 at any scale, and the ability to compare entropy levels across scales within person. We argue
122 that a clarification of these issues is thus necessary for valid inferences of time scale-specific
123 ‘neural irregularity’ in a growing number of neuroscientific MSE applications.

124 **Issue 1: Global similarity bounds introduce a scale-dependent variance bias**

125 A principle assumption of sample entropy is that “the degree of irregularity of a complex
126 signal [...] cannot be entirely captured by the SD [i.e., standard deviation]” [24; i.e., square root
127 of variance]. To ensure this, sample entropy is typically assessed relative to the standard
128 deviation of the broadband signal to intuitively normalize the estimation of irregularity for
129 overall distributional width [9, 10, see also 24]. In particular, the *similarity bound* – defined by
130 a constant r , by which the signal SD is multiplied – reflects the tolerance for labeling time points
131 as being similar or different, and thus, determines how liberal the algorithm is towards detecting
132 ‘matching patterns’ (Fig 2A-C). While wider bounds decrease entropy estimates, narrower
133 bounds increase them [9, 25, 26] (S2 Figure). Crucially, the similarity bound is often not equally
134 liberal across time scales, resulting in an entropy estimation bias. Specifically, to characterize
135 temporal irregularity at coarser time scales, signals are typically successively low-pass filtered
136 [or ‘coarse-grained’; 27] (Fig 2D), whereas the similarity bound typically (in its ‘Original’
137 implementation) is set only once – namely relative to the SD of the original unfiltered signal.
138 Due to the progressive filtering, coarse-graining successively removes variance from the signal,
139 yet a single global (i.e., scale-invariant) similarity bound remains based on the cumulative
140 variance of all estimable frequencies (Fig 2D and E). As a result, the similarity bound becomes
141 increasingly liberal towards pattern similarity at coarser scales, thereby reducing entropy
142 estimates. This is most clearly illustrated by the observation that white noise signals, which
143 should be characterized as equally random at each time scale, exhibit decreasing entropy values
144 towards coarser scales when global *similarity bounds* are used [23, 25, 28]. This issue has been
145 recognized previously [25], and provided a rationale for recomputing the *similarity bound* for
146 each time scale [25, 29]. But despite the benefits of this refinement that was already proposed
147 fifteen years ago, our review of the literature revealed that the use of global bounds remains

148 dominant in over 90% of neuroscientific MSE applications (see S1 File) and in previous
 149 validation work [23]. Thus, we argue that a comprehensive assessment of the resulting bias is
 150 needed to highlight this issue, both to clarify previous results and to guide future studies.
 151

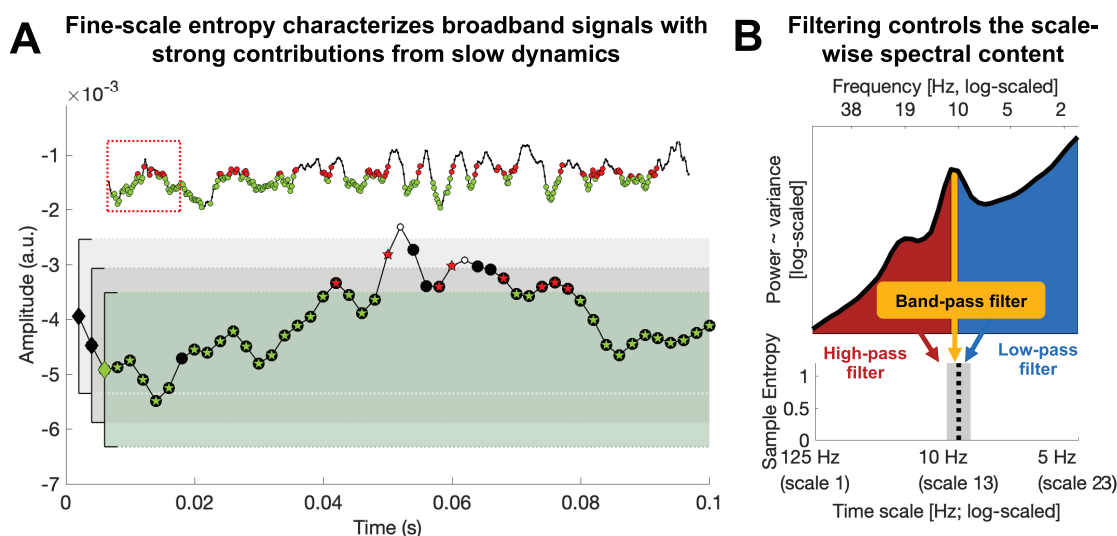


152
 153 **Fig 2.** Issue 1: Global similarity bounds systematically confound the entropy of coarse-scale signals with removed
 154 spectral power. (A, B) Similarity bounds constrain sample entropy as shown schematically for entropy estimation
 155 using narrower (A) and wider (B) similarity bounds. For clarity, only a subset of pattern matches (green ticks) and
 156 mismatches (red cross) are indicated for a sequence length $m = 1$ (cf. Fig 1B). Wider, more liberal similarity bounds
 157 indicate more pattern matches than narrow, conservative bounds, thereby decreasing entropy. S2 Figure shows the
 158 empirical link between liberal similarity bounds and sample entropy estimates. (C-E) Divergence between global
 159 similarity bounds and scale-wise signal SD biases coarse-scale entropy. (C) Coarse-graining (see Figure 1A)
 160 progressively reduces variance from the original broadband signal (as shown in panel E). (D) At original sampling
 161 rates (i.e., time scale 1; marked red in panels DE and F), neural signal variance is usually composed of broadband
 162 1/f content and narrowband rhythmic peaks. Note that the x-axis plots decreasing frequencies to align with the
 163 traditional MSE low-pass filter direction. Towards coarser scales (e.g., scale 30; marked blue in CD and E), signal
 164 variance progressively decreases, as the signal becomes more specific to low frequencies. (E) Due to the systematic
 165 and cumulative reduction of variance in scale-wise signals, global similarity bounds become liberally biased
 166 ('broad'). Critically, systematic differences in the magnitude of this bias (e.g., due to different spectral slopes)
 167 introduce systematic entropy differences at coarser scales.

168 **Issue 2: Traditional scale definitions lead to diffuse time scale reflections of spectral**
 169 **content**

170 While matched similarity bounds account for *total signal variation* at any specific time
 171 scale, sample entropy remains related to *the variance structure* (i.e., the power spectrum) of the
 172 signal as *one* indicator of its temporal irregularity [4]. Most neural signals exhibit a scale-free
 173 $\frac{1}{f^x}$ power distribution [30, 31], for which the exponent x indicates the prevalence of low-to-
 174 high-frequency components in the signal. This ratio is also referred to as the power spectral

175 density (PSD) slope. Smaller exponents (indicating shallower PSD slopes) characterize signals
 176 with relatively strong high-frequency contributions (i.e., reduced temporal autocorrelations,
 177 and less predictability) compared to larger exponents indicating steeper slopes. This conceptual
 178 link between PSD slopes and sample entropy has been empirically observed both across
 179 subjects and wakefulness states [10, 13, 32]. However, the sensitivity of fine-scale entropy to
 180 PSD slopes – a multi-scale characteristic – highlights that the contribution of slow-to-fast signal
 181 content to fine-scale entropy is unclear. This ambiguity arises from the algorithm that derives
 182 scale-wise signals. In particular, ‘Original’ MSE implementations use low-pass filters to derive
 183 signals at coarser time scales, which increasingly constrains entropy estimates to slower
 184 fluctuations. However, the opposite is not true. Hence, finer time scales characterize the *entire*
 185 broadband signal (see Fig 3A) which represents a non-specific mixture of both low and high
 186 frequency elements [33, 34]. Crucially, the contribution of these elements to neural broadband
 187 signals is not equal. Rather, the variance of $\frac{1}{f^x}$ signals is dominated by the amplitude of low
 188 frequencies, which may thus disproportionately impact the assessment of pattern irregularity. As
 189 a result, broadband signal characterization challenges the assumption that fine-scale entropy
 190 mainly describes ‘fast’ events. More generally, this highlights large uncertainty regarding the
 191 frequencies that are represented at *any* particular time scale.
 192



193
 194 **Fig 3.** Issue 2: Traditional scale derivation leads to diffuse time-scale reflections of spectral power. (A) Exemplary
 195 sample entropy estimation in the same empirical EEG signal shown in Fig 1B, but without application of a high-
 196 pass filter, thus including dominant slow dynamics. See Figure 1B for a legend of the Figure elements. In brief,
 197 green elements indicate pattern matches at $m+1$, whereas red elements indicate pattern mismatches at $m+1$. In the
 198 presence of large low-frequency fluctuations, sample entropy at fine scales (here scale 1) may to a large extent
 199 characterize the temporal regularity of slow dynamics. Note that this is not a case of biased similarity bounds, but
 200 a desired adjustment to the large amplitude of slow fluctuations. The inset shows an extended segment (800 ms)
 201 of the same signal, allowing for an assessment of the slower signal dynamics. The red box indicates the 100 ms
 202 signal shown in the main plot. (B) A scale-wise filter implementation controls the scale-wise spectral content,
 203 as schematically shown here for the filter-dependent representation of spectral content at a time scale of
 204 approximately 10 Hz (for a note on the x-axis labeling, see methods: *Calculation of multi-scale sample entropy*).
 205 Traditionally, low-pass filters are used to derive coarser scales, which introduces a sensitivity to slower
 206 fluctuations. However, other filter implementations can be used to e.g., investigate the pattern irregularity of fast
 207 signal variations. No matter whether low or high pass filters are used, the spectral content influencing entropy

208 estimates is by definition not specific to any particular time scale; band-pass filters provide one viable solution
209 permitting such specificity.

210

211 Narrowband rhythmic structure projected into simulated noise signals [1, 30, 35] provides
212 a well-controlled situation in which to study the mapping of neural irregularity to MSE time
213 scales, due to their clearly defined time scale (i.e., period = inverse of frequency) and regularity
214 (added rhythmic variance = more regular signal = decreased entropy). Moreover, rhythmic
215 structure remains a dominant target signal in neuroscience for which entropy, as a
216 complementary descriptor, should provide an anti-correlated reflection. However, previous
217 simulations on the mapping of rhythms onto MSE time scales have produced puzzling results
218 that have received little attention in the literature so far; while a linear mapping between
219 rhythmic frequency and entropy time scales has been observed, added rhythmic regularity has
220 been shown to *increase* entropy above baseline in previous work [4, 18, 36]. This notably
221 contrasts with the intuition that added signal regularity should reduce observed entropy. Thus,
222 additional simulations are necessary to assess the intuitive notion that rhythmicity should be
223 anticorrelated with entropy, and to investigate whether this phenomenon indeed occurs at
224 specific time scales, as previously assumed [4, 18, 36]. In particular, we probed the feasibility
225 of using high-pass and band-pass filters (relative to standard low-pass options) to control the
226 MSE time scales at which rhythmicity would be reflected (Fig 3B).

227 In summary, Issue 1 suggests a coarse-scale bias introduced by global similarity bounds,
228 and Issue 2 highlights broadband contributions to fine scales. In worst-case scenarios, a
229 conjunction of these issues may lead to a reflection of fast dynamics in coarse entropy and a
230 reflection of slow dynamics in fine entropy, thus paradoxically *inverting* the intuitive time scale
231 interpretation. These issues have not been jointly assessed, however, and there is little evidence
232 on the significance of these methodological issues for practical inferences.

233 **Impact of issues on practical inferences: age differences in neural irregularity at fast** 234 **and slow time scales**

235 One principal application of multiscale entropy is in the domain of lifespan covariations
236 between neural dynamics and structural brain network ontogeny [for a review see 37]. Within
237 this line of inquiry, it has been proposed that structural brain alterations across the lifespan
238 manifest as entropy differences at distinct time scales [12, 14, 32, 38]. Specifically, it has been
239 suggested that coarse-scale entropy decreases and fine-scale entropy rises with increasing adult
240 age as a reflection of senescent shifts from global to increasingly local information processing
241 [12, 14]. Crucially, this mirrors observations based on spectral power, where age-related
242 decreases in the magnitude of low-frequencies [39, 40] are accompanied by increases in high-
243 frequency activity, conceptualized also as a flattening of power spectral density (PSD) slopes
244 [12, 14, 32, 41]. These results seemingly converge towards a joint decrease of low-frequency
245 power and coarse-scale entropy in older adults (and an increase for both regarding fast
246 dynamics). However, this correspondence is surprising upon closer inspection given the
247 presumed anticorrelation between the magnitude of signal regularity (as indicated by spectral
248 power) and entropy. Given concerns regarding the interpretation of entropy time scales, we
249 assessed cross-sectional age effects on both MSE and spectral power as a test case for potential
250 mismatches in scale-dependent inferences.

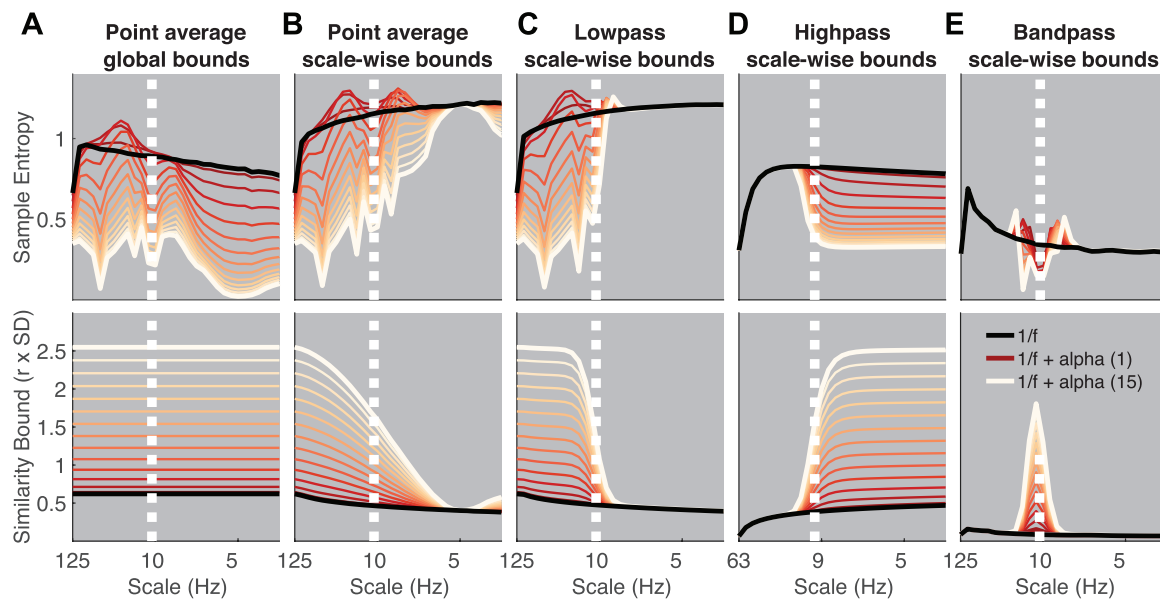
251 **Current study**

252 Here, we aimed to address two issues of frequency-to-scale mapping and their relevance
253 for empirical applications. First, we simulated variations in rhythmic power and frequency to
254 probe the relationship between rhythmicity and MSE time scales. Primarily, our goal was to
255 assess how global similarity bounds (Issue 1) and the scale-wise spectral content of the analyzed
256 signal (Issue 2) influence the time scales at which added rhythmicity is observed. Then, we
257 attempted to replicate reported cross-sectional age differences in human
258 electroencephalography (EEG) signals recorded during rest. We assessed whether younger
259 adults would show increased coarse scale and decreased fine-scale entropy compared to older
260 adults, and we probed the extent to which such scale-specific results depend on mismatched
261 spectral power via the issues above. Finally, we probed the possibility of deriving ‘frequency-
262 specific’ estimates of signal irregularity, and assessed age differences therein. We refer to
263 traditional settings that use global bounds and low-pass filtering as ‘Original’ throughout the
264 remainder of the manuscript (see methods for details).

265 **Results**

266 **Simulations indicate a diffuse mapping between rhythmicity and MSE time scales as a** 267 **function of global similarity bounds and spectral signal content**

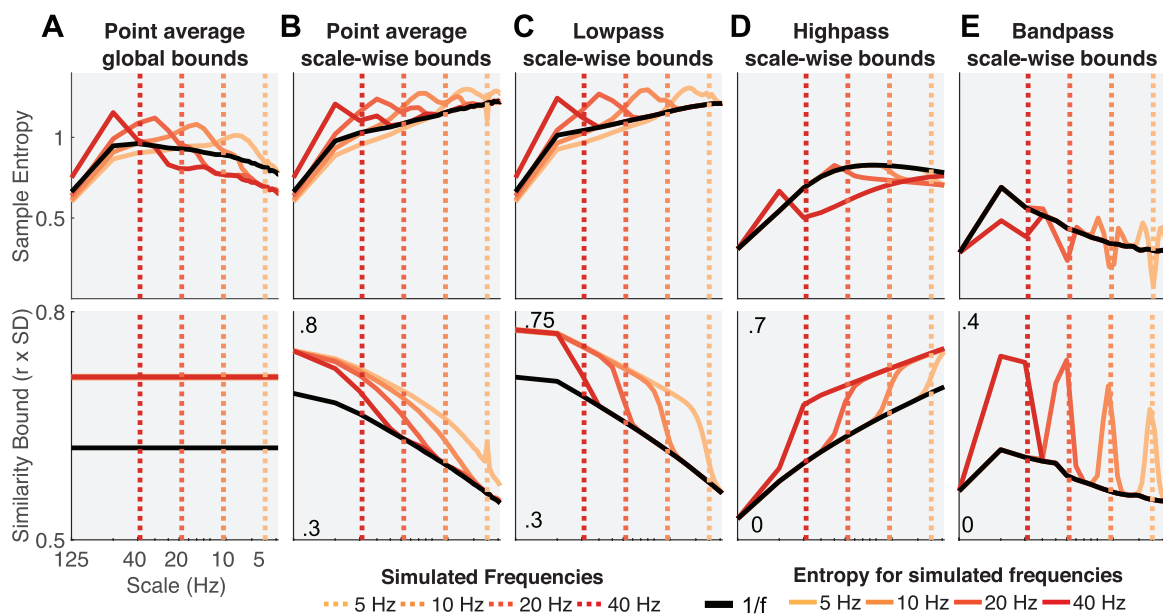
268 Our first aim was to probe how scale-specific events, namely rhythms of a given frequency,
269 modulate MSE time scales. For this purpose, we simulated 10 Hz (alpha) rhythms of varying
270 power on top of pink noise and calculated the MSE of those signals. First, we probed the
271 influence of global similarity bounds (as used in ‘Original’ implementations) on the time scale
272 mapping (Issue 1). Crucially, as a result of using a global similarity bound for all time scales,
273 strong rhythmic power decreased MSE estimates across a range of time scales, including time
274 scales at which added 10 Hz rhythmicity did not contribute to the scale-wise signal (Fig 4A,
275 upper panel). As highlighted in Issue 1, this can be explained by a general increase in the
276 liberality of bounds (Fig 4A, lower panel) that introduced a bias on coarse-scale entropy below
277 10 Hz. In contrast, when scale-dependent similarity bounds were used with low-pass filters (Fig
278 4BC), strong rhythmicity systematically affected entropy only at finer time scales than the
279 simulated frequency (i.e., to the left of the vertical line in Fig 4C, albeit in a diffuse manner,
280 which we will examine next).



281
 282 **Fig 4. Rhythmic power manifests at different time scales depending on filter choice and similarity bound.**
 283 Simulations indicate at which time scales the addition of varying magnitudes of stereotypic narrowband 10 Hz
 284 rhythms (blue-to-red line gradient) modulate entropy compared to the baseline 1/f signal (black line). Simulations
 285 indicate that increases in rhythmicity strongly reduce entropy estimates alongside increases in the similarity bound.
 286 The affected scales vary as a function of global vs. scale-dependent similarity bounds and the spectral filtering
 287 used to derive coarser time scales. Crucially, in ‘Original’ implementations, added narrowband rhythmicity
 288 decreased entropy with low scale-specificity, in line with global increases in the similarity bound (A). In contrast,
 289 the use of scale-varying thresholds (B) and dedicated filtering (C-E) increased specificity regarding the time scales
 290 at which rhythmicity was reflected. Note that timescales are presented in Hz to facilitate the visual assessment of
 291 rhythmic modulation. For all versions except high pass, the scale represents the upper Nyquist bound of the
 292 embedding dimension. For the high pass variant, the scale represents the high pass frequency (see methods). Time
 293 scales are log-scaled. Spectral attenuation properties of the Butterworth filters are shown in S4 Figure.

294 Second, we assessed the influence of the scale-wise filters (and hence, the spectral signal
 295 content) on frequency-to-scale mapping (see Issue 2, Fig 3B). In particular, we expected that
 296 low-pass filters (A-C) would lead to entropy decreases at finer time scales than the simulated
 297 frequency, whereas high-pass filters would lead to a rhythm representation at coarser time
 298 scales (Fig 3B). In line with these expectations, low-pass filters constrained the influence of
 299 narrowband rhythms to finer time scales (Fig 4C). As in previous work [29], Butterworth filters
 300 (Fig 4C) improved the removal of 10 Hz rhythms at coarser time scales and produced less
 301 aliasing compared with ‘Original’ point-averaging (see methods, Fig 4AB), with otherwise
 302 comparable results. Hence, low-pass filters rendered multiscale entropy sensitive to variance
 303 from low frequencies, suggesting that slow events (e.g. event-related potentials) are reflected
 304 in a diffuse manner across time scales. In contrast, high-pass filters constrained rhythm-induced
 305 entropy decreases to coarser time scales that included 10 Hz signal content, hence leading to
 306 estimates of high frequency entropy that were independent of low frequency power (Fig 4D).
 307 Finally, when band-pass filters were used (Fig 4E), rhythmicity decreased sample entropy at
 308 the target scales (despite producing edge artifacts surrounding the time scale of rhythmicity).
 309 In sum, these analyses highlight that rhythmic power increases will diffusely and non-
 310 specifically modulate MSE time scales as a function of the coarse-graining filter choice, unless
 311 a narrowband filter is applied.

312 Such diffuse reflection of rhythms across MSE time scales is at odds with previous
 313 simulations suggesting a rather constrained, linear mapping between the frequency of simulated
 314 rhythms and entropy time scales [4, 18, 36]. Furthermore, those studies indicated entropy
 315 *increases* with added rhythmicity, in contrast with the marked (and expected) decreases in
 316 entropy observed here. Crucially, increased entropy relative to baseline runs counter to the idea
 317 that the addition of a stereotypic pattern should decrease rather than increase pattern
 318 irregularity. To assess whether these seemingly divergent results can be reconciled, we repeated
 319 our simulation for different frequencies. We focused on a comparatively low level of
 320 rhythmicity (amplitude level = 2; SNR ~ 1.3 (see methods); S3 Figure displays exemplary time
 321 series), for which Fig 4A-C suggested transient entropy increases above baseline. Similar to
 322 previous reports, we observed a positive association between simulated frequencies and peak
 323 entropy time scales (Fig 5) across implementations, such that rhythms of a given frequency
 324 increased entropy at slightly finer time scales (see increases in entropy above baseline to the
 325 left of the dotted vertical lines in Fig 5A-C). However, as shown in Fig 4A-C, such increases
 326 were counteracted when rhythmic strength increased, while global *similarity bounds* (Fig 5A)
 327 liberally biased, and thus decreased, entropy at coarser time scales (i.e., to the right of the dotted
 328 lines in Fig 5A) independent of rhythmic strength. While the mechanistic origin of entropy
 329 increases remains unclear, previous conclusions may thus have overemphasized the scale-
 330 specificity of rhythmic influences.
 331



332
 333 **Fig 5. Influence of rhythmic frequency on MSE estimates and similarity bounds across different MSE**
 334 **variants.** Simulations of different frequencies indicate a linear frequency-to-scale mapping of simulated sinusoids.
 335 Broken vertical lines indicate the simulated frequency. Low-pass MSE variants show increased entropy at time
 336 scales finer than the simulated frequency in combination with a global entropy decrease. Low-, high- and band-
 337 pass variants exhibit the properties observed in the alpha case, with a reduction above/below or at the simulated
 338 frequency. Time scales are log-scaled.

339 In sum, our simulations highlight that the choice of similarity bound and the signal's spectral
 340 content grossly affect one's ability to interpret MSE time scales. Our frequency-resolved

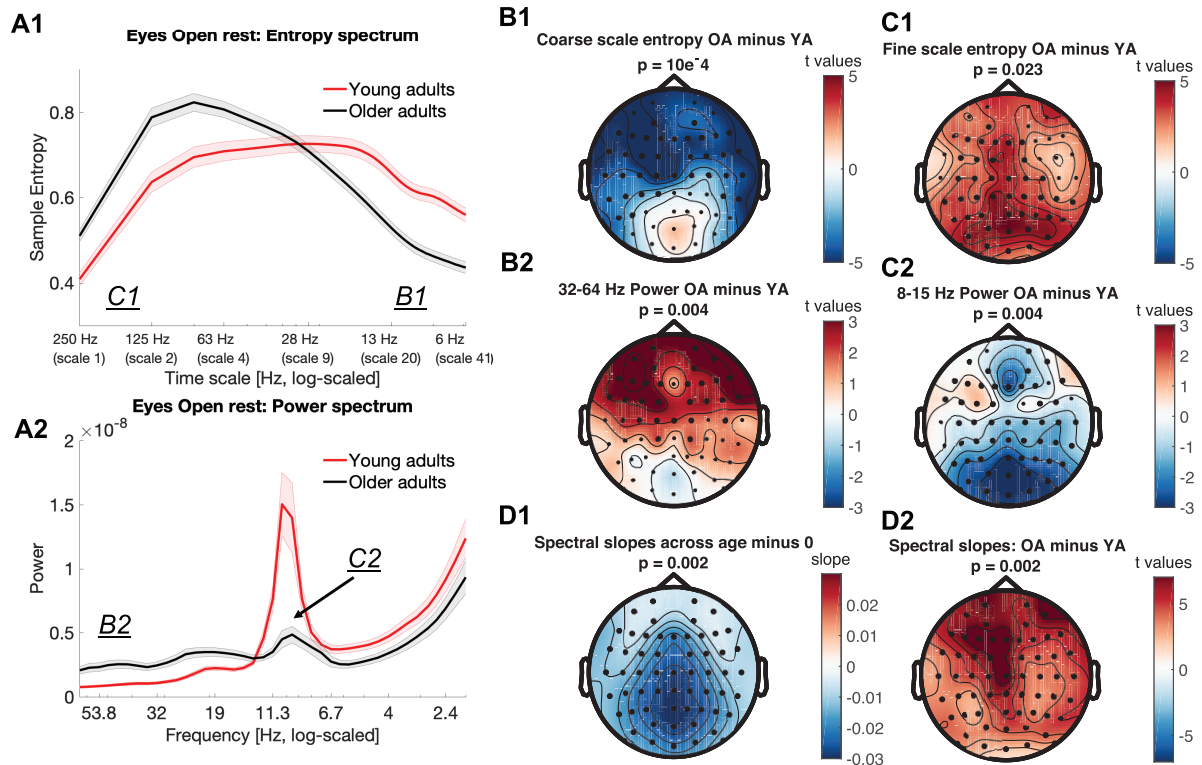
341 simulations suggest that a previously argued direct frequency-to-scale mapping is not tenable
342 when typical estimation procedures are used.

343 **Probing the impact of spectral power on MSE in a cross-sectional age comparison**

344 Our simulations suggest profound influences of the choice of similarity bound (Issue 1) and
345 spectral content (Issue 2) on scale-dependent MSE estimates. However, whether these issues
346 affect inferences in empirical data remains unclear. Entropy differences across the lifespan are
347 an important application [6], where ‘Original’ MSE implementations suggest that older adults
348 exhibit higher entropy at finer time scales and lower entropy at coarser time scales compared
349 to younger adults [for a review see 37]. Importantly, a shallowing of PSD slopes with age has
350 also been reported, as represented by higher power at high frequencies and lower power at low
351 frequencies [32, 41]. The raised issues of a potential (1) reflection of high frequency power on
352 coarse scales and (2) diffuse reflection of slow spectral content thus question whether traditional
353 MSE group differences reflect veridical differences in signal irregularity at matching time
354 scales. Given those two issues, we specifically hypothesized that:

- 355
- 356 (A) Adult age differences in coarse-scale MSE can be accounted for by group differences in
357 high frequency power, due to the typical use of global similarity bounds (Issue 1).
 - 358 (B) Adult age differences in fine-scale MSE reflect differences in PSD slopes and thus depend
359 on the contribution of low frequencies to broadband signals (Issue 2).
- 360

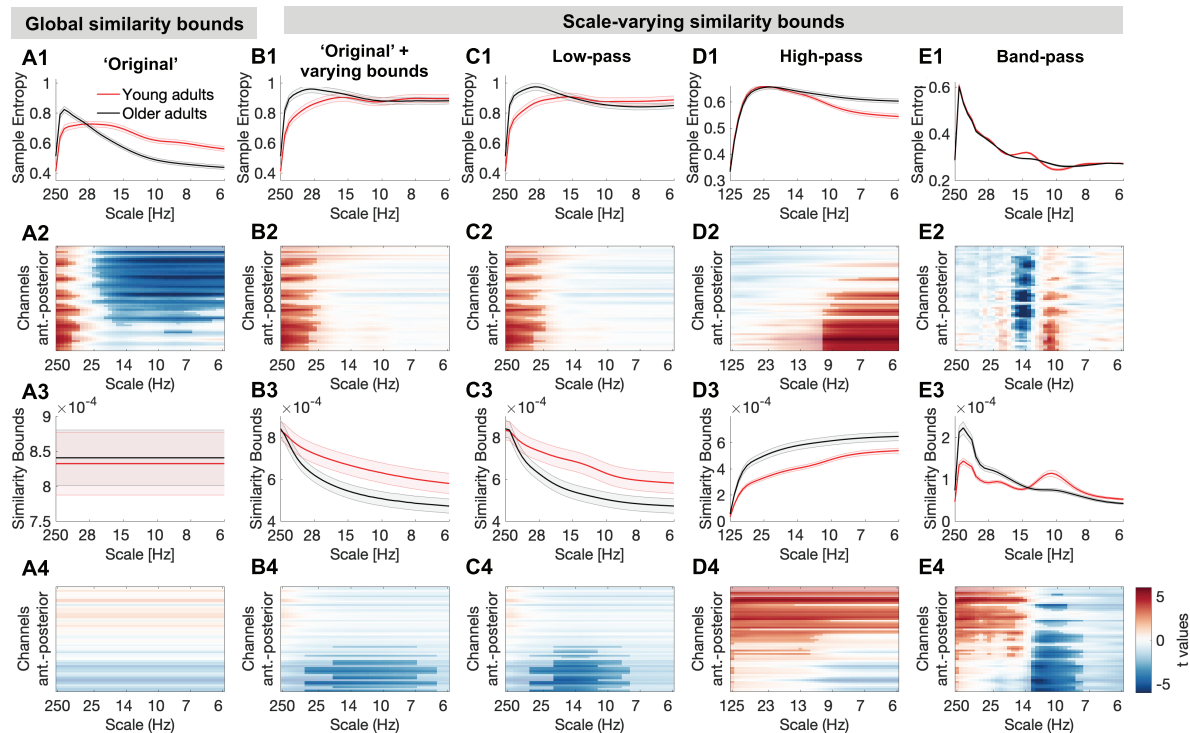
361 To assess these hypotheses, we first attempted to replicate previously reported scale-wise
362 age differences in MSE and spectral power during eyes open rest. ‘Original’ settings replicated
363 scale-dependent entropy age differences (Fig 6A1). Specifically, compared with younger
364 adults, older adults exhibited lower entropy at coarse scales, and higher entropy at fine scales
365 (Fig 6A1). Mirroring these results in spectral power, older adults had lower parieto-occipital
366 alpha power and increased frontal high frequency power (Fig 6A2) compared to younger adults.
367 This was globally associated with a shift from steeper to shallower PSD slopes with increasing
368 age (Fig 6D). At face value, this suggests joint shifts of both power and entropy, in the same
369 direction and at matching time scales. Crucially, however, the spatial topography of entropy
370 differences inverted the time scale of power differences (Fig 6B & C; cf., upper and lower
371 topographies), such that frontal high frequency power topographies resembled coarse entropy
372 topographies (Fig 6B), while parieto-occipital age differences in slow frequency power
373 resembled fine-scale entropy differences (Fig 6D). This rather suggests scale-mismatched
374 associations between entropy and power.



375
 376 **Fig 6. Timescale-dependent age differences in spectral power and entropy during eyes open rest.** (A) MSE
 377 (A1) and power (A2) spectra for the two age groups. Error bars show standard errors of the mean. Note that in
 378 contrast to standard presentations of power, the log-scaled x-axis in A2 is sorted by decreasing frequency to enable
 379 a better visual comparison with entropy time scales (see also Fig 2D). T-values of power age contrast are shown
 380 in S5 Figure. (B, C) Topographies of age differences indicate mirrored age differences in fast entropy and low
 381 frequency power, as well as coarse entropy and high frequency power. Significant differences are indicated by
 382 asterisks. (D1) Spectral slopes across age groups. (D2) Age differences in spectral slopes.

383 Next, we assessed the impact of scale-wise similarity bounds and different scale-wise filters
 384 on the indication of MSE age differences (Fig 7).

385



386
 387 **Fig 7. Multiscale entropy age differences depend on the specifics of the estimation method.** Grand average
 388 traces of entropy (1st row) and similarity bounds (3rd row) alongside t-maps from statistical contrasts of age
 389 differences (2nd + 4th row). Age differences were assessed by means of cluster-based permutation tests and are
 390 indicated via opacity. Original MSE (A) replicated reported scale-dependent age differences, with older adults
 391 exhibiting higher entropy at fine scales and lower entropy at coarse scales, compared with younger adults. The
 392 coarse-scale difference was exclusively observed when using global similarity bounds, whereas the fine-scale age
 393 difference was indicated with all low-pass versions (A, B, C), but not when signals were constrained to high-
 394 frequency or narrow-band ranges (D, E). In contrast, narrowband MSE indicated inverted age differences within
 395 the alpha and beta band (E).

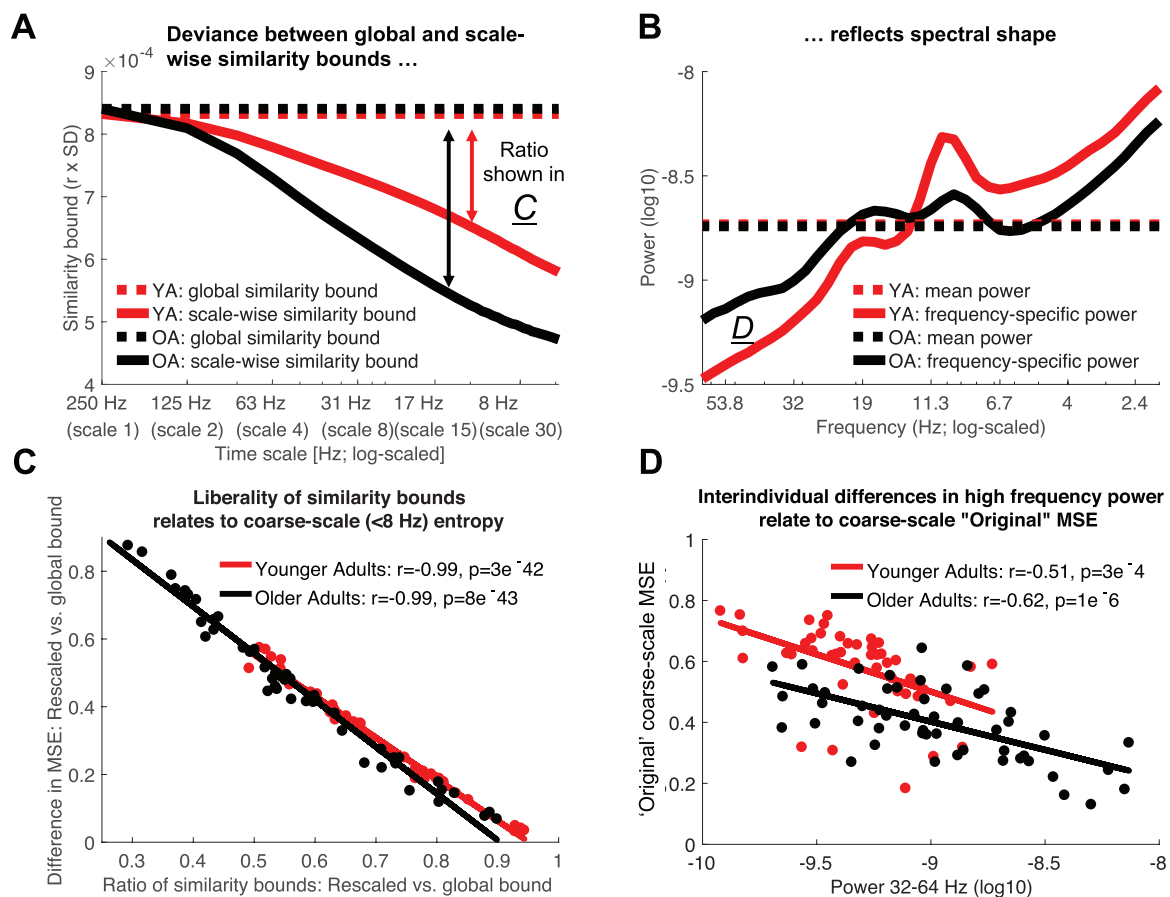
396
 397 Briefly, we observed three main results that deserve highlighting:
 398

- 399 (A) The implementation of scale-wise similarity bounds affected MSE age differences (Fig 7;
 400 Hypothesis A; Issue 1). In particular, with global bounds, MSE indicated increased fine-
 401 scale and decreased coarse-scale entropy for older compared to younger adults (Fig 7A1
 402 and A2), in the absence of group differences in the global *similarity bound* (Fig 7A3 and
 403 A4). In contrast, scale-varying bounds captured age differences in variance at finer scales
 404 (Fig 7B) and abolished age differences in coarse-scale entropy (effect size was significantly
 405 reduced from $r = .58$ to $r = .07$; $p = 6.8 \times 10^{-5}$; see Statistical analyses).
 406 (B) The chosen scale-wise filtering method also affected MSE age differences (Hypothesis B;
 407 Issue 2). Specifically, fine-scale entropy age differences were indicated when low-pass
 408 filters rendered those scales sensitive to low-frequency content (Fig 7B/C). Effect size did
 409 not significantly change with the adoption of scale-varying similarity bounds (from $r = .44$
 410 to $r = .45$; $p = .934$). In contrast, when high-pass filters constrained fine scales to high
 411 frequency signals (Fig 7D), no fine-scale age differences were observed and the age effect
 412 was significantly reduced to $r = .09$ ($p = .008$).

413 (C) Strikingly, the implementation of narrowband filters (Fig 7E) indicated two unique age
 414 effects not recoverable using other approaches: larger 'narrowband' alpha-band entropy
 415 and lower beta-band entropy for older adults compared with younger adults.
 416
 417 In the following sections, we assess these results more closely.

418 Global similarity bounds bias coarse-scale entropy to reflect high-frequency power

419 Scale-dependent entropy effects in the face of global similarity bounds (as observed in the
 420 'Original' implementation; Fig 7A) may intuitively suggest scale-specific variations in signal
 421 irregularity in the absence of variance differences. However, global similarity bounds
 422 increasingly diverge from the scale-wise signal variance towards coarser scales (Issue 1; Fig
 423 8A). This introduces a liberal bias that systematically varies as a function of the removed
 424 variance, thereby rendering coarse MSE scales sensitive to differences in higher frequency
 425 power (i.e., Issue 1), as observed in the case of aging (Fig 8A & B).
 426



427
 428 **Fig 8. Divergence of scale-specific signal variance from global similarity bounds accounts for age differences**
 429 **in coarse-scale entropy.** (A, B) A global similarity bound does not reflect the spectral shape, thus leading to
 430 disproportionally liberal criteria at coarse scales following the successive removal of high-frequency variance (see
 431 Fig 2D-F for the schematic example). Scale-dependent variance is more quickly reduced in older compared to
 432 younger adults (A) due to the removal of more prevalent high-frequency variance in the older group (B). This
 433 leads to a differential bias across age groups, as reflected in the differentially mismatched distance between global
 434 and scale-dependent similarity bounds at coarser scales. (C) Removing this bias by adjusting the similarity bounds
 435 to the scale-dependent signal is associated with increases in coarse-scale entropy. This shift is more pronounced

436 in older adults following the removal of a more prevalent bias. (D) With global similarity bounds, coarse-scale
437 entropy strongly reflects high frequency power due to the proportionally more liberal similarity threshold
438 associated. Low frequency power < 8 Hz was not consistently related to coarse-scale entropy (log10-power as in
439 D; YA: $r = .12$; $p = .419$; OA: $r = .36$, $p = .009$). Data in A and B are global averages, data in C and D are averages
440 from frontal Original effect cluster (see Fig 4B) at entropy time scales below 6 Hz.

441 To assess whether global bounds introduced an association between high frequency
442 power and coarse scale entropy in the case of aging, we probed changes in *similarity bounds*
443 and MSE between the use of global and scale-varying bounds. As expected, we observed a
444 strong anti-correlation between inter-individual changes in *similarity bounds* and MSE (Fig
445 8C). That is, the more similarity bounds were re-adjusted to match the scale-wise variance, the
446 more entropy estimates increased. Crucially, this difference was more pronounced for older
447 adults (paired t-test; r : $p = 5e-6$; MSE: $p = 3e-4$). Due to their increased high frequency power,
448 coarse-graining decreased older adults' scale-wise variance more so than younger adults'
449 variance. Thus, global similarity bounds presented a more liberal threshold at coarser scales for
450 older adults than for younger adults, in turn producing lower MSE estimates. In line with this
451 assumed link between high frequency power and coarse scale entropy as a function of global
452 bounds, individual high frequency power at frontal channels was anticorrelated with coarse-
453 scale entropy estimates when a global similarity bound was applied (Fig 8D), but was
454 dramatically weaker when the similarity bound was recomputed for each scale (YA: $r = -0.15$;
455 $p = .302$; OA: $r = .20$, $p = .146$). This is in line with our observation that coarse-scale age
456 differences (Fig 7A) were not found when scale-wise bounds were used (Fig 7B).

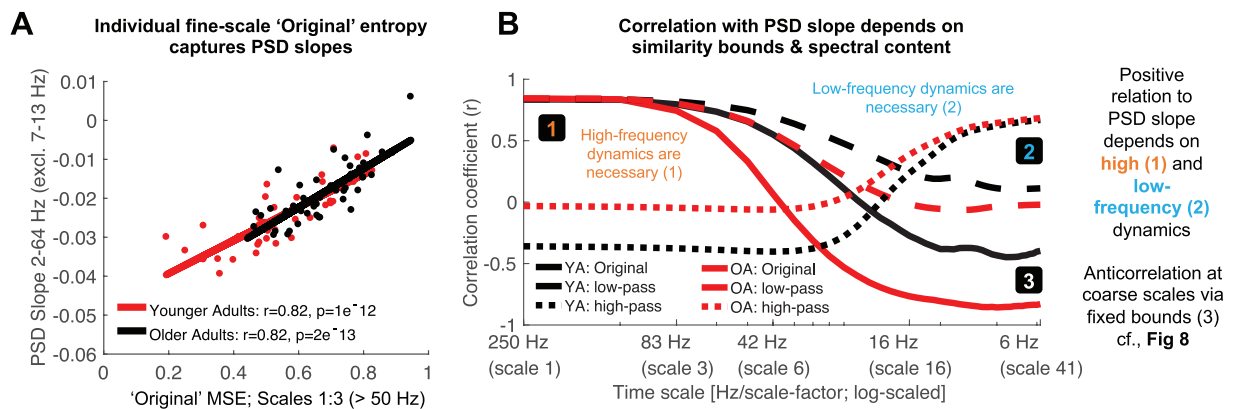
457 Taken together, these results indicate that increased high frequency power with age can
458 account for entropy decreases at coarse time scales, whereas the pattern irregularity of slow
459 dynamics *per se* was not modulated by age.

460 **Low-frequency contributions render fine-scale entropy a proxy measure of PSD slope**

461 A common observation in the MSE literature is that MSE is highly sensitive to task and
462 behavioral differences at fine time scales, which are assumed to reflect fast dynamics. This is
463 surprising given that high-frequency activity remains challenging to measure [42]. Moreover,
464 previous studies suggest that fine-scale entropy reflects power spectral density (PSD) slopes
465 [e.g., 10, 32]. Given that 'Original' MSE implementations contain both high- and low-
466 frequency components due to the assessment of broadband signals, we probed whether fine-
467 scale associations with PSD slopes depend on the presence of slow fluctuations and whether
468 age-related slope variations can account for fine-scale entropy age differences (Hypothesis B).

469 As expected, individual fine-scale entropy was strongly and positively related to PSD slopes
470 (Fig 9A) in both younger and older adults. Notably, after high-pass filtering the signal, the
471 positive relation of fine-scale entropy to PSD slopes disappeared in both age groups (Fig 9B,
472 dotted lines), and turned negative in older adults (see S6 Figure), while age differences in fine-
473 scale entropy disappeared (Fig 7D). Relations between entropy and PSD slopes – and age
474 differences – re-emerged once low-frequency content was included in the entropy estimation
475 (Fig 9C, dashed lines), indicating that the presence of slow fluctuations was necessary for PSD
476 slope relations. To assess whether varying PSD slopes accounted for fine-scale age differences
477 in 'Original' MSE, we computed partial correlations between the measures. No significant

478 prediction of age group status by fine-scale entropy was observed when controlling for the high
 479 collinearity with PSD slopes ($r = -.06$, $p = .59$), whereas PSD slopes significantly predicted age
 480 group status when controlling for MSE ($r = .38$, $p < .001$).



481
 482 **Fig 9. The presence of low- and high-frequency content renders fine entropy slopes sensitive to PSD slopes.**
 483 A) Sample entropy at fine time scales represents the slope of power spectral density across age groups. The 7-13
 484 Hz range was excluded prior to the PSD slope fit to exclude the rhythmic alpha peak (see Fig 8B). (B) The presence
 485 of both slow and fast dynamics is required for positive associations with PSD slopes to emerge. The direction and
 486 magnitude of correlations of scale-wise entropy with PSD slopes depends on the choice of global vs. rescaled
 487 similarity bounds, as well as the choice of filtering. Original entropy inverts from a positive correlation with PSD
 488 slope at fine scales to a negative association at coarse scales. Rescaling of the similarity bound abolishes the
 489 negative correlation of coarse-scale entropy with PSD slopes. S6 Figure presents scatter plots of these
 490 relationships. The x-axis indicates the upper frequency bounds for the low-pass version.

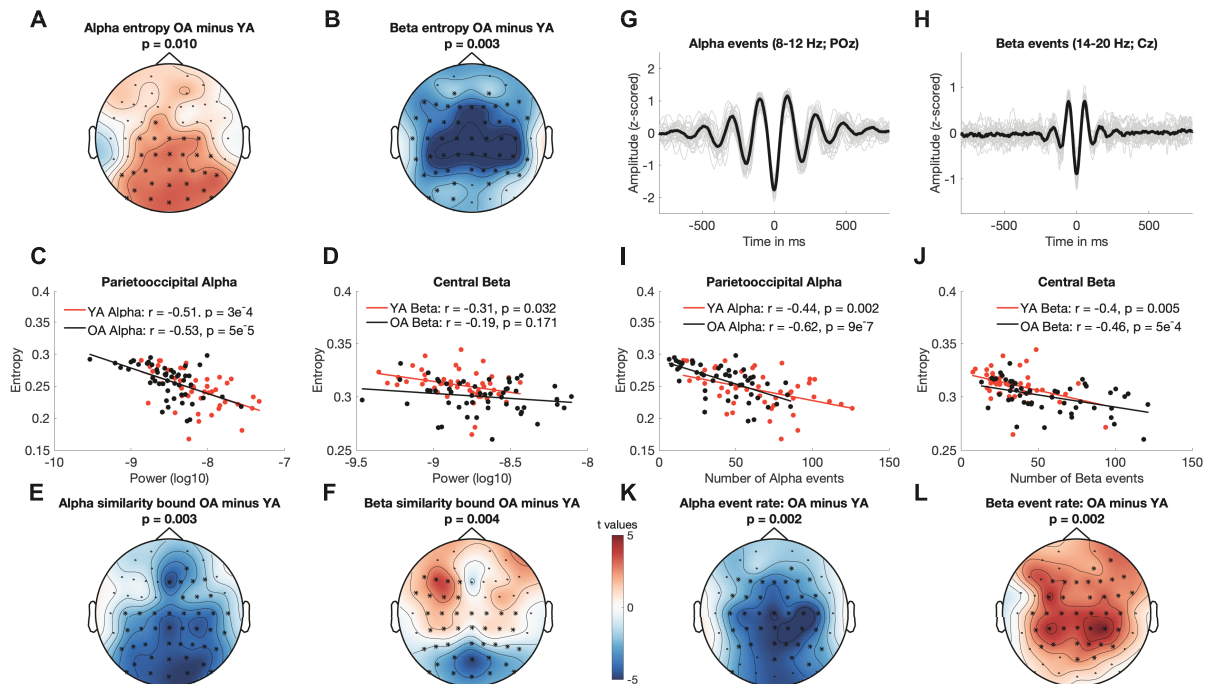
491
 492 Finally, spectral slopes were anticorrelated with coarse-scale entropy when global similarity
 493 bounds were used (Fig 9C, solid lines), but not when criteria were scale-wise re-estimated (Fig
 494 9C, dashed and dotted lines). This again suggests a presence of the scale-wise bias noted in
 495 Issue 1 (i.e., scale-wise bound divergence); subjects with shallower slopes (more high
 496 frequency power) had increasingly liberally-biased thresholds at coarser scales, resulting in
 497 overly low entropy estimates.

498 In sum, age differences in fine-scale entropy were conditional on the presence of both low-
 499 and high-frequency dynamics and reflected differences in PSD slopes; while the pattern
 500 irregularity of fast dynamics *per se* was not modulated by age.

501 **Narrowband MSE indicates age differences in signal irregularity in alpha and beta band**

502 The previous analyses highlighted how the spectral content of the signal can give rise to
 503 MSE time scale mismatches. However, our simulations also suggest a far more accurate
 504 mapping between entropy and power when scale-wise bandpass filters are used (Fig 4A).
 505 Concurrently, application of the band-pass implementation indicates a partial decoupling
 506 between entropy and variance (as reflected in the *similarity bound*) age differences (Fig 7E).
 507 Specifically, older adults exhibited higher parieto-occipital entropy at alpha time scales (~8-12
 508 Hz) and lower central entropy at beta time scales (~12-20 Hz) than in younger adults (Fig 7; Fig
 509 10AB). Whereas alpha-band entropy was moderately and inversely correlated with alpha power
 510 (Fig 10C) and the age difference was inversely reflected in the similarity bound in a
 511 topographically similar fashion (Fig 10E), the same was not observed for entropy in the beta
 512 range for both age groups (Fig 10DF). Promisingly, this indicates evidence for what many who

513 employ MSE measures in cognitive neuroscience presume – that power and entropy *can* be
 514 decoupled, providing complementary signatures of neural dynamics.
 515



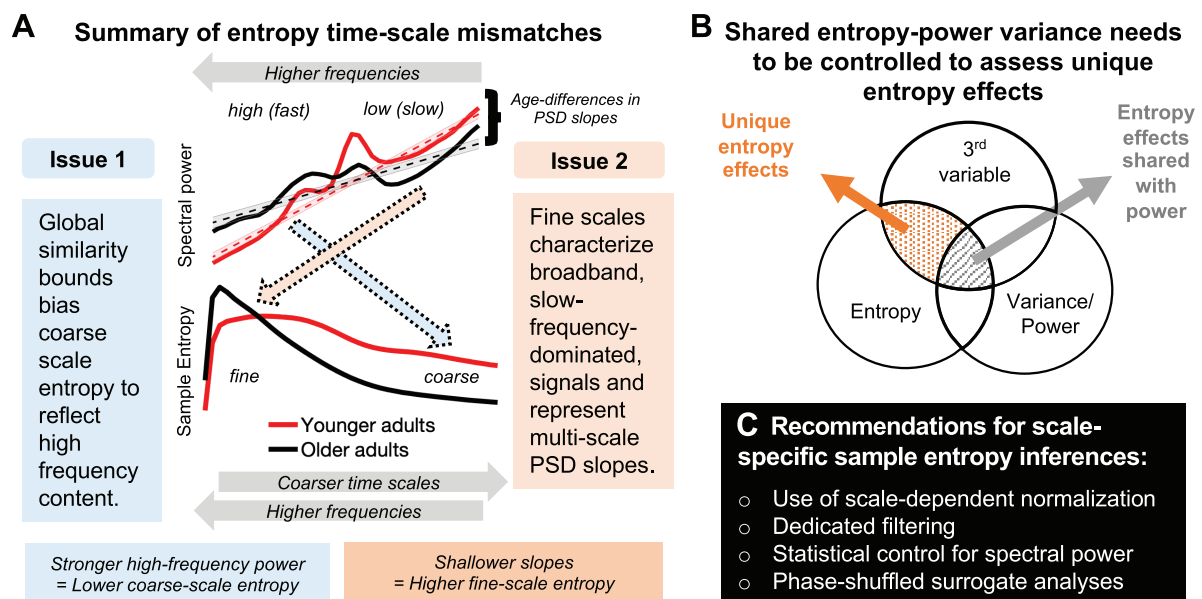
516
 517 **Fig 10. Narrowband MSE reflects age differences in alpha- and beta-specific event (ir)regularity.** (A, B)
 518 Narrowband MSE indicates age differences in the pattern complexity at alpha (A) and beta (B) frequencies. (C, D)
 519 Alpha, but not beta power consistently correlates negatively with individual narrowband entropy within clusters
 520 of age differences. (E, F) Similarly, alpha but not beta similarity bounds show an inverted age effect with similar
 521 topography. (G, H) Single-trial rhythm detection highlights a more transient appearance of beta compared with
 522 alpha events. (I, J) The rate of stereotypical single-trial alpha and beta events is anticorrelated with individual
 523 narrowband entropy. (K, L) The rate of spectral events exhibits age differences that mirror those observed for
 524 entropy.

525 This divergence of entropy and power in the beta band is particularly interesting as beta
 526 events have been observed to exhibit a more transient waveform shape [43, 44], while
 527 occupying a lower total duration during rest than alpha rhythms [34]. Indeed, it should be the
 528 rate of stereotypic spectral events that reduces pattern irregularity rather than the overall power
 529 within a frequency band. To better test this assumption in our data, we applied single-trial
 530 rhythm detection to extract the individual rate of alpha (8-12 Hz) and beta (14-20 Hz) events.
 531 As predicted, alpha events had a more sustained appearance compared with beta events as
 532 shown in Fig 10G & H (events were time-locked to the trough of individual events; see
 533 methods). Importantly, both alpha and beta event rate were inversely and moderately correlated
 534 with entropy estimates (Fig 10IJ) at matching time scales in the band-pass version. Correlations
 535 were also numerically higher than between power and entropy (Fig 10C and D), suggesting that
 536 entropy captured the non-stationary character of the rhythmic episodes that are not captured by
 537 sustained power estimates. The relationships remained stable after controlling for individual
 538 event rate and entropy in the age effect cluster of the other frequency band (partial correlations:
 539 alpha for younger adults: $r = -.52$, $p = 2e-4$; alpha for older adults: $r = -.71$, $p = 8e-9$; beta for
 540 younger adults $r = -.49$, $p = 6e-4$; beta for older adults: $r = -.56$, $p = 2e-5$), indicating separable
 541 associations between event rate and entropy between the two frequency bands. This is
 542 important, as our simulations suggest increased entropy estimates around narrow-band filtered

543 rhythmicity (see Fig 4A). Furthermore, a permutation test indicated age differences in beta rate
 544 that were opposite in sign to the entropy age difference (see Fig 10L). In particular, older adults
 545 had a higher number of central beta events during the resting state compared with younger
 546 adults, thus rendering their beta-band dynamics more stereotypic. In sum, these results suggest
 547 that narrowband MSE estimates approximate the irregularity of non-stationary spectral events
 548 at matching time scales.

549 Discussion

550 MSE aims to characterize the temporal irregularity of (neural) time series at multiple
 551 temporal scales. In the present study, we have highlighted two primary issues that may render
 552 the interpretation of time scales unintuitive in traditional applications: (Issue 1) biases from
 553 global similarity bounds, and; (Issue 2) the characterization of broadband, low-frequency
 554 dominated signals (see Fig 11A for a schematic summary). In the following, we discuss these
 555 effects and how they can impact traditional inferences regarding signal irregularity, in particular
 556 with regard to empirical age differences. Then, we discuss age effects in narrowband signal
 557 irregularity at interpretable temporal scales. Finally, we recommend procedures to improve
 558 scale-specific MSE inferences.
 559



560
 561 **Fig 11. Summary of the identified time-scale mismatches and recommendations for future studies.** (A) We
 562 highlight two scale-dependent mismatches that run counter to the intuition that entropy at fine scales primarily
 563 refers to fast dynamics, and vice-versa: (1) Coarse-scale entropy is biased towards reflecting high-frequency
 564 content when signals of decreasing variance are compared to a global, and increasingly inadequate, similarity
 565 bound. (2) Fine-scale entropy characterizes scale-free 1/f slopes when broadband signals include slow frequency
 566 content. (B) Beyond time-scale mismatches, entropy and variance can often be collinear, in part due to their shared
 567 description of linear signal characteristics, such as rhythmicity. To identify complementary and unique relations
 568 of pattern complexity compared to more established measures of variance, explicit statistical control is required
 569 for the latter. (C) We propose multiple strategies to safeguard future applications against the highlighted issues.

570

571 **Issue 1: Global similarity bounds bias coarse-scale entropy estimates**

572 Coarse scale entropy is commonly thought to represent the irregularity of slow dynamics.
573 However, MSE's traditionally global similarity bounds systematically bias coarse scale entropy
574 estimates. Given that scale-wise variance decreases across scales, the liberality of global
575 similarity bounds increases, causing entropy to decrease despite no ostensible shift in pattern
576 irregularity. This bias is independent of the values of the global similarity bound – which did
577 not differ across groups here – but rather depends on the *removed* variance at the time scale of
578 interest. This issue has led to puzzling results in past work. For example, several papers using
579 typical forms of ('original') MSE have shown that in white noise signals (which by definition
580 should be equally irregular at all time scales), entropy appears to unintuitively decrease towards
581 coarser scales, whereas pink noise signals undergo less entropy reduction across initial scales
582 due to the removal of less high-frequency content [25]. Strikingly, such puzzling effects have
583 been used to *validate* the most common implementation of MSE [e.g., 23, 28] rather than to
584 indicate the presence of a systematic bias in estimation. This appears motivated by the
585 assumption that “changes of the variance due to the coarse-graining procedure are related to the
586 temporal structure of the original time series, and should be accounted for by the entropy
587 measure” [8]. We rather consider the similarity bound divergence as a clear bias for the intuitive
588 interpretation of time scales in MSE applications.

589 Importantly, this bias affects practical inferences. In the current resting-state EEG data, an
590 age-related increase in high frequency power manifested unintuitively as a decrease in coarse-
591 scale entropy via systematic group differences in the divergence of similarity bounds. Note that
592 we presume that this age difference arises from a relative bias. As such, variations in high-
593 frequency power suffice, even at low levels in 1/f scenarios, to systematically impact coarse-
594 scale estimates and to specifically explain variance in a third variable of interest (e.g., age; see
595 Fig 11B). Given that global similarity bounds remain prevalent in applications (see S1 File),
596 we hope that our practical example motivates the adoption of scale-varying parameters. Overall,
597 we perceive little justification for the use of scale-invariant parameters in MSE estimation in
598 future work.

599 **Issue 2: Fine-scale entropy relates to PSD slopes in the presence of slow frequency** 600 **content**

601 While fine-scale entropy is often interpreted as a signature of “fast” temporal irregularity,
602 it is typically estimated from broadband signals. As such, fine (or single) scale entropy has been
603 proposed as a signature of desynchronized cortical states [32, 45] that feature a suppression of
604 low-frequency power with concurrent increases in the magnitude of high frequency dynamics
605 [46-48]. This synergy is thought to benefit local information processing by regulating cortical
606 gain as a function of the local excitation-inhibition (E/I) balance. Spectral (PSD) slopes,
607 characterizing the scale-free ‘background’ or ‘noise’ component of the total variance, and have
608 been proposed as an index of such E/I balance [41, 49, 50]. By linking fine-scale entropy to
609 PSD slopes, we replicated previous observations of increasing fine-scale entropy with
610 shallower slopes [10, 13, 25, 32, 51] and shorter temporal autocorrelations [4, 23, 52]. However,

611 we qualify this association by highlighting that the *joint* presence of slow and fast dynamics in
612 the signal is necessary to produce such effects.

613 The association between broadband signal entropy and spectral slopes coheres with the
614 notion that shallower slopes have a more ‘noisy’ or irregular appearance in the time domain.
615 Thus, spectral slopes and temporal irregularity may be conceptualized – at least in part – as
616 different perspectives on the same signal characteristics. Practically however, the
617 correspondence between fine-scale entropy and 1/f slopes should nonetheless be tested, given
618 that these scales are also sensitive to other signals characteristics, such as narrowband
619 rhythmicity (as shown in our simulations). In sum, our analyses provide insights into the
620 sensitivity of fine-scale entropy to desynchronized cortical states and highlight the surprising
621 importance of slow fluctuations for such associations.

622 **Spectral power and entropy: What’s irregularity got to do with it?**

623 For entropy to be a practical and non-redundant measure in cognitive neuroscience, both its
624 convergent and discriminant validity to known signal characteristics should be established.
625 Multiple features can influence the temporal irregularity of neural time series. These include
626 traditional ‘linear’ PSD features, (e.g., temporal autocorrelation, rhythmicity, etc.) as well as
627 ‘non-linear’ features (e.g., phase resets, cross-frequency coupling, etc.). It is therefore worth
628 noting that associations between spectral power characteristics and entropy estimates are partly
629 anticipated (Fig 11B). For example, as noted before, entropy should reduce with increased
630 rhythmic irregularity, and increase with shallowing of PSD slopes (and hence, shortening of
631 temporal autocorrelations). However, the use of MSE is often motivated by its perceived
632 sensitivity to non-linear properties of brain dynamics that cannot be captured by traditional PSD
633 analyses [e.g., 53, 54, 55]. In extreme cases, an independence between estimates may
634 sometimes be erroneously inferred from the use of variance-based similarity bounds. Contrary
635 to such orthogonality assumptions, our analyses highlight that differences in spectral variance
636 (as captured by the similarity bound, which is typically neglected as a measure of interest when
637 estimating MSE) may account for a large proportion of reported MSE effects [see also appendix
638 in 23]. As such, non-linear characteristics *per se* may often do little to drive MSE estimates.

639 **Relevance of identified time scale mismatches to previous work**

640 Although the highlighted issues broadly apply to applications in which MSE is a measure
641 of interest (e.g., assessment of clinical outcomes [e.g., 18]; prediction of cognitive performance
642 [e.g., 38]), our results are also especially relevant for MSE differences across the lifespan.
643 Previous applications indicated that older adults exhibit lower coarse-scale entropy and higher
644 fine-scale entropy compared with younger adults [12, 14, 23]. In the power spectrum, these
645 effects were inverted, with older subjects showing enhanced high-, and reduced low-frequency
646 power. This was previously taken as evidence that older adults’ high-frequency dynamics were
647 not only enhanced in magnitude, but also more unpredictable compared with younger adults’
648 dynamics. While we replicate similar results here when standard MSE implementation are
649 applied, our analyses question the validity of previous interpretations. In particular, our results
650 suggest that age-related increases in coarse-scale entropy do not reflect differences in the

651 irregularity of slow dynamics, but rather reflect differential high frequency power. An absence
652 of age differences at coarse scales is in line with previous work with scale-wise similarity
653 bounds [15]. Similarly, our analyses indicate that differences in fine-scale ‘pattern irregularity’
654 describe age-related changes in PSD slopes, which themselves reflect a shift from distributed
655 to local processing. Taken together, our results suggest that entropy age differences dominantly
656 arise from differences in the PSD spectrum, and appear at counterintuitive time scales. This is
657 further in line with a previous application using surrogate data that highlighted that age group
658 differences were mainly captured by linear auto-correlative properties [see appendix in 23].

659 **Cross-sectional age differences in narrowband MSE**

660 Complementing traditional broadband applications, our use of narrowband MSE suggested
661 age-related entropy increases in the posterior-occipital alpha band and decreases in central beta
662 entropy that inversely tracked the regularity of alpha and beta events, respectively. Posterior-
663 occipital decreases in alpha power and frequency with age are fundamental findings in many
664 age-comparative studies [56]. While age-related increases in beta power are not observed as
665 consistently [see e.g., 56 for a review], age-related increases in their prevalence have been
666 observed during eyes open rest [57]. In addition, beta power increases over contralateral motor
667 cortex during rest may reflect greater GABAergic inhibition in healthy aging [58]. While our
668 results are not hemisphere-specific, they may similarly reflect increased inhibition in older
669 adults, potentially reflected in an increased number of stereotypical beta events [44]. As our
670 aims were methods-focused in the present study, the functional interpretation of our observed
671 age differences necessitates caution pending further research. Nevertheless, these results
672 highlight that scale-specific narrowband filtering can provide novel, frequency-specific,
673 insights into event/signal irregularity.

674 **Recommendations for future applications**

675 The issues raised here suggest that additional steps need to be taken to achieve valid scale-
676 wise estimates of MSE, and to support the perceived complementary nature of MSE relative to
677 more typical measures (such as spectral power, etc.):

- 678 a) We see little motivation for the use of global similarity bounds as they introduce challenges
679 rather than benefits. We therefore recommend the field abandons global *similarity bounds*
680 in MSE applications.
- 681 b) We recommend spectral filters to validate the scale-specificity of effects. For example, if
682 effects are observed at fine temporal scales with a low-pass filter, additional high-pass
683 filters may inform about the spectral extent of the effect. For entropy estimates of slow
684 dynamics, traditional low-pass filter settings already apply this principle by becoming
685 increasingly exclusive to slow fluctuations (if scale-dependent normalization is used). If the
686 signal is filtered into dedicated frequency ranges, inferences regarding pattern irregularity
687 become narrowband-specific. While this narrowband entropy by definition enforces a more
688 rhythmic appearance than the raw signal may convey [59] and thus cannot capture multi-
689 scale properties at any single scale, it may nevertheless provide a complementary index of
690 frequency-specific variability.

- 691 c) We regard statistical control as necessary to establish entropy effects that are not capturable
692 by traditional linear indices (such as PSD characteristics). While some studies have shown
693 joint effects of interest in MSE and (band-limited) spectral power [11, 12, 14, 15, 60-66],
694 others identified unique MSE effects [18, 67-69]. However, the (mis)match between time-
695 scales and frequencies may not always be readily apparent, at least in part due to the various
696 issues raised here. As shown here, controls should include both narrowband (‘rhythmic’)
697 power and the arrhythmic signal background. As the scale-wise *similarity bound* is used for
698 normalization, it should at the very least be controlled for. The choice of features may
699 further be aided by comparing effect topographies of spectral power and entropy, as done
700 in the present study. An important point to note is the relevance of statistical controls for
701 relations to third variables (see Fig 11B). While some studies highlight scale-dependent
702 associations of entropy with power, a large amount of shared variance (e.g., of coarse-scale
703 entropy with slow frequency power) does not guarantee that a smaller portion of residual
704 variance (e.g., shared with normalization biases) systematically does or does not relate to
705 other effects of interest. This is equally relevant for identifying unique non-linear
706 contributions. For example, while we observed moderate associations between band-
707 specific rhythm events and entropy here, this non-redundant association nevertheless leaves
708 room for the two measures to diverge in relation to third variables. This is in line with prior
709 work [23, 70] showing that despite a dominant influence of linear characteristics on entropy
710 estimates, non-linear contributions can uniquely explain a (smaller) portion of entropy
711 variance.
- 712 d) Finally, a principled way to dissociate non-linear signal characteristics from linear signal
713 variance is to use phase-shuffled surrogate data [5, 71-74]. Phase randomization effectively
714 alters original time series patterns while preserving linear PSD characteristics and “is
715 unavoidable if conclusions are to be drawn about the existence of nonlinear dynamics in the
716 underlying system” [5]. While such surrogate approaches have been utilized in select
717 entropy applications [4, e.g., appendix of 23] to highlight entropy’s non-linear sensitivity
718 [e.g., 26, 28], it has not become common practice in application. Given that spectral power
719 can impact MSE in many ways, of which some are shown here, we consider surrogate
720 analyses as an optimal approach to verify the contribution of non-linear signal
721 characteristics.

722
723 In combination, such controls may go a long way toward establishing unique, complementary,
724 and valid contributions of MSE in future work.

725 **Conclusions**

726 Many inferences regarding multiscale entropy in cognitive/clinical neuroscience rely on the
727 assumption that estimates uniquely relate to pattern irregularity at specific temporal scales. Here
728 we show that both assumptions may be invalid depending on the consideration of signal
729 normalization and spectral content. Using simulations and empirical examples, we showed how
730 spectral power differences can introduce entropy effects that are inversely mapped in time scale
731 (i.e., differences in the high frequency power may be reflected in coarse entropy and vice versa;
732 see Fig 11A). As these results suggest fundamental challenges to traditional MSE analysis

733 procedures and inferences, we highlight the need to test for unique entropy effects (Fig 11B)
734 and recommend best practices and sanity checks (Fig 11C) to increase confidence in the
735 complementary value of pattern irregularity for cognitive/clinical neuroscience. While the
736 warranted claim has been made that “it would be unreasonable simply to reduce sample entropy
737 to autocorrelation, spectral power, non-stationarity or any of their combinations” [4], this
738 should not mean that we cannot test whether one or more of these contributors may sufficiently
739 explain MSE effects of interest. We thus propose that MSE effects may be taken as a starting
740 point to explore the linear and nonlinear features of brain signals [e.g., 76]. We believe that
741 empirical identification of the unique predictive utility of MSE will advance the quest for
742 reliable mechanistic indicators of flexible brain function across the lifespan, and in relation to
743 cognition, health, and disease.

744 **Methods**

745 **Simulations of relations between rhythmic frequency, amplitude, and MSE**

746 To assess the influence of rhythmicity on entropy estimates, we simulated varying
747 amplitudes (0 to 7 arbitrary units in steps of 0.5) of 10 Hz (alpha) rhythms on a fixed 1/f
748 background. This range varies from the absence to the clear presence of rhythmicity (see S3
749 Figure for an example). The background consisted of $\frac{1}{f^x}$ -filtered Gaussian white noise (mean =
750 0; std = 1) with $x = 1$ that was generated using the function `f_alpha_gaussian` [77]. The
751 background was additionally band-pass filtered between .5 and 70 Hz using 4th order
752 Butterworth filters. Eight second segments (250 Hz sampling rate) were simulated for 100
753 artificial, background-varying trials, and phase-locked 10 Hz sinusoids were superimposed. To
754 analyze the reflection of rhythmic frequency on time scales and to replicate a previously
755 observed linear frequency-to-timescale mapping between the spectral and entropy domains [4,
756 18, 36], we repeated our simulations with sinusoids of different frequencies (5 Hz, 10 Hz, 20
757 Hz, 40 Hz, 80 Hz), that covered the entire eight second-long segments. For a specified
758 amplitude level, the magnitude of frequency-specific power increases (or narrowband signal-
759 to-noise ratio) increased alongside simulated frequencies due to the decreasing frequency power
760 of pink noise, while the ratio of rhythmic-to-global signal variance (or global signal-to-noise
761 ratio (SNR)) remained constant across simulated frequencies. We used the following definition:
762 $SNR_{global} = \left(\frac{RMS_{signal}}{RMS_{noise}}\right)^2$, where RMS_{noise} is the root mean square of the pink noise time series
763 and RMS_{signal} characterizes the pink noise signal with added rhythmicity.

764 **Resting state data and preprocessing**

765 To investigate the influence of similarity bounds and filter ranges in empirical data, we used
766 resting-state EEG data collected in the context of a larger assessment prior to task performance
767 and immediately following electrode preparation. Following exclusion of three subjects due to
768 recording errors, the final sample contained 47 younger (mean age = 25.8 years, SD = 4.6, range
769 18 to 35 years; 25 women) and 52 older adults (mean age = 68.7 years, SD = 4.2, range 59 to
770 78 years; 28 women) recruited from the participant database of the Max Planck Institute for

771 Human Development, Berlin, Germany (MPIB). Participants were right-handed, as assessed
772 with a modified version of the Edinburgh Handedness Inventory [78], and had normal or
773 corrected-to-normal vision. Participants reported to be in good health with no known history of
774 neurological or psychiatric incidences, and were paid for their participation (10 € per hour). All
775 older adults had Mini Mental State Examination (MMSE) [79, 80] scores above 25. All
776 participants gave written informed consent according to the institutional guidelines of the
777 Deutsche Gesellschaft für Psychologie (DGPS) ethics board, which approved the study.

778 Participants were seated at a distance of 80 cm in front of a 60 Hz LCD monitor in an
779 acoustically and electrically shielded chamber. Following electrode placement, participants
780 were instructed to rest for 3 minutes with their eyes open and closed, respectively. During the
781 eyes open interval, subjects were instructed to fixate on a centrally presented fixation cross. An
782 auditory beep indicated to the subjects when to close their eyes. Only data from the eyes open
783 resting state were analyzed here. EEG was continuously recorded from 64 active (Ag/AgCl)
784 electrodes using BrainAmp amplifiers (Brain Products GmbH, Gilching, Germany). Sixty scalp
785 electrodes were arranged within an elastic cap (EASYCAP GmbH, Herrsching, Germany)
786 according to the 10% system [81], with the ground placed at AFz. To monitor eye movements,
787 two electrodes were placed on the outer canthi (horizontal EOG) and one electrode below the
788 left eye (vertical EOG). During recording, all electrodes were referenced to the right mastoid
789 electrode, while the left mastoid electrode was recorded as an additional channel. Online,
790 signals were digitized at a sampling rate of 1 kHz.

791 Preprocessing and analysis of EEG data were conducted with the FieldTrip toolbox [82]
792 and using custom-written MATLAB (The MathWorks Inc., Natick, MA, USA) code. Offline,
793 EEG data were filtered using a 4th order Butterworth filter with a pass-band of 0.2 to 125 Hz.
794 Subsequently, data were downsampled to 500 Hz and all channels were re-referenced to
795 mathematically averaged mastoids. Blink, movement and heart-beat artifacts were identified
796 using Independent Component Analysis [ICA; 83] and removed from the signal. Artifact-
797 contaminated channels (determined across epochs) were automatically detected using (a) the
798 FASTER algorithm [84], and by (b) detecting outliers exceeding three standard deviations of
799 the kurtosis of the distribution of power values in each epoch within low (0.2-2 Hz) or high (30-
800 100 Hz) frequency bands, respectively. Rejected channels were interpolated using spherical
801 splines [85]. Subsequently, noisy epochs were likewise excluded based on FASTER and on
802 recursive outlier detection. Finally, recordings were segmented to participant cues to open their
803 eyes, and were epoched into non-overlapping 3 second pseudo-trials. To enhance spatial
804 specificity, scalp current density estimates were derived via 4th order spherical splines [85]
805 using a standard 10-05 channel layout (conductivity: 0.33 S/m; regularization: 1^{-05} ; 14th
806 degree polynomials).

807 **Calculation of (modified) multi-scale sample entropy (mMSE)**

808 MSE characterizes signal irregularity at multiple time scales by estimating sample
809 entropy (SampEn) at each time scale of interest. A schematic of the estimation pipeline is shown
810 in S1 Figure. The mMSE code is provided at <https://github.com/LNDG/mMSE>. A tutorial for
811 computing mMSE has been published on the FieldTrip website
812 (http://www.fieldtriptoolbox.org/example/entropy_analysis/).

813 **Sample entropy estimation procedure.** The estimation of SampEn involves counting how
814 often patterns of m successive data points reoccur in time (\mathbf{p}^m) and assessing how many of
815 those patterns remain similar when the next sample $m+1$ is added to the sequence (\mathbf{p}^{m+1}). Given
816 that amplitude values are rarely exactly equal in physiological time series, a *similarity bound*
817 defines which individual data points are considered similar. This step discretizes the data and
818 allows to compare data patterns rather than exact data values. The similarity bound is defined
819 as a proportion r of the time series standard deviation (SD ; i.e., square root of signal variance)
820 to normalize the estimation of sample entropy for total signal variation. That is, for any data
821 point k , all data points within $k \pm r \times SD$ are by definition equal to k , which forms the basis for
822 assessing sequence patterns. SampEn is finally given as the natural log of $\mathbf{p}^m(r)/\mathbf{p}^{m+1}(r)$.
823 Consequently, high SampEn values indicate low temporal regularity as many patterns of length
824 m are not repeated at length $m+1$. In our applications, m was set to 2 and r was set to .5, in line
825 with prior recommendations [9] and EEG applications [23, 38, 86].

826 **Multi-scale signal derivation procedure.** To extend sample entropy to multiple time scales,
827 MSE ‘coarse-grains’ the original time series for multiple scale factors τ (here 1 to 42, where 1
828 refers to the original signal). The ‘Original’ MSE method [7, 8] averages time points within
829 non-overlapping time bins (i.e., ‘point averaging’). Such point averaging is equivalent to a low-
830 pass finite-impulse response (FIR) filter, which can introduce aliasing however [29, 87] and
831 constrains the specificity towards increasingly slow signals, while not allowing specificity to
832 fast dynamics or any particular frequency range of interest. To implement control over the
833 scale-wise filter direction and to reduce aliasing, we applied either low- [27, 29, 87], high-, or
834 band-pass filters at each scale factor. The low-pass cut-off was defined as $LP = \frac{1}{scale} * nyquist$
835 and was implemented using a 6th order Butterworth filter. Similarly, the high-pass cut-off was
836 defined as $HP = \frac{1}{scale+1} * nyquist$, implemented via 6th order Butterworth filters. Note that
837 these cut-offs describe the upper and lower frequency bounds at each time scale, respectively.
838 Finally, band-pass filters were applied to obtain narrowband estimates by sequentially applying
839 Chebyshev Type I low- and high-pass filters (4th order with passband ripple of 1dB; chosen to
840 achieve a fast filter roll-off), thus ensuring that each scale captured frequency-specific
841 information. The passband was defined as $BP = LP \pm 0.05 * LP$. To avoid pronounced passband
842 ripple for broad passbands, 10th order Butterworth filters replaced the Chebyshev filters at
843 scales where the passband was larger than $0.5 * Nyquist$. At scale 1, only a high-pass 10th order
844 Butterworth filter was applied as the sampling rate of the signal set the upper (Nyquist)
845 frequency bound. These settings were chosen to optimize the pass-through of signals within the
846 pass-band and the attenuation of signals outside the pass-band. Two-pass filtering using
847 MATLAB’s `filtfilt` function was applied to achieve zero-phase delay. S4 Figure shows the
848 spectral attenuation properties [88] of the filters. To avoid edge artefacts, input signals were
849 symmetrically mean-padded with half the pseudo-trial duration (i.e., 1500 ms). After filtering,
850 we implemented a point-skipping procedure to down-sample scale-wise signals (see S1 Figure).
851 Since point-skipping allows for increasing starting point permutations k for increasing scale
852 factors τ , we counted patterns separately for each starting point k , summed the counts of pattern
853 matches and non-matches across them, and computed sample entropy based on the summed
854 counts as described above: $MSE(\mathbf{x}, \tau, \mathbf{m}, \mathbf{r}) = \ln\left(\frac{\sum_{k=1}^{\tau} \mathbf{p}^m}{\sum_{k=1}^{\tau} \mathbf{p}^{m+1}}\right)$. This implementation is equivalent

855 to “refined composite MSE” [89] and can improve the stability of entropy results for short or
856 noisy signals [27, 89]. Note that no point skipping was performed in the ‘high-pass’
857 implementation to avoid low-pass filtering. As a result, the signals at increasing scale factors
858 remained at the original sampling rate. To alleviate computational cost, scale factors were
859 sampled in step sizes of 3 for empirical data (only for the ‘high-pass’ implementation) and later
860 spline-interpolated. An adapted version of MSE calculations was used for all settings [90], in
861 which scale-wise entropy was estimated across discontinuous data segments. The estimation of
862 scale-wise entropy across trials allows for reliable estimation of coarse-scale entropy without
863 requiring long, continuous signals, while quickly converging with estimates from continuous
864 segments [90].

865 **Multi-scale calculation of similarity bounds.** Following scale-specific filtering, all
866 implementations re-calculated sample entropy for the scale-specific signal. Crucially, in
867 ‘Original’ applications [7, 8], the *similarity bound* is calculated only once from the original
868 broadband signal. As a result of filtering, the scale-wise signal SD decreases relative to the
869 global, scale-invariant similarity bound [25]. To overcome this limitation, we recomputed the
870 similarity bound for each scale factor, thereby normalizing MSE with respect to changes in
871 overall time series variation at each scale ($.5 \times$ SD of scale-wise signal).

872 **Scale factor notation.** As the interpretation of estimates at each scale is bound to the scale-
873 wise spectral content, our Figures indicate spectral bounds of the scale-wise signals alongside
874 the scale factor as follows: for the low- and band-pass implementation, we indicate the low-
875 pass frequency as calculated above as the highest resolvable (i.e., Nyquist) frequency in the
876 scale-specific signal. Likewise, for the high-pass implementation, we indicate the high-pass
877 limit as the lowest resolvable frequency in the scale-specific signal. In the main text, we refer
878 to higher scale factors as ‘coarser’ scales’ and lower scale factors as ‘finer’ scales, in line with
879 the common use in the literature. Note that the sampling rate of the simulated data was 250 Hz,
880 whereas the empirical data had a sampling rate of 500 Hz.

881 **Calculation of power spectral density (PSD)**

882 Power spectral density estimates were computed by means of a Fast Fourier Transform
883 (FFT) over 3 second pseudo-trials for 41 logarithmically spaced frequencies between 2 and 64
884 Hz (employing a Hanning-taper; segments zero-padded to 10 seconds) and subsequently
885 averaged. Spectral power was \log_{10} -transformed to render power values more normally
886 distributed across subjects. Power spectral density (PSD) slopes were derived by linearly
887 regressing power values on log-transformed frequencies. The spectral range from 7-13 Hz was
888 excluded from the background fit to exclude a bias by the narrowband alpha peak [32, 41].

889 **Detection of single-trial spectral events**

890 Spectral power, even in the narrowband case, is unspecific to the occurrence of
891 systematic rhythmic events as it also characterizes periods of absent rhythmicity [e.g., 91].
892 Specifically detecting rhythmic episodes in the ongoing signal alleviates this problem, as
893 periods of absent rhythmicity are excluded. To investigate the potential relation between the

894 occurrence of stereotypic spectral events and narrowband entropy, we detected single-trial
895 spectral events using the extended BOSC method [34, 92, 93] and probed their relation to
896 individual entropy estimates. In short, this method identifies stereotypic ‘rhythmic’ events at
897 the single-trial level, with the assumption that such events have significantly higher power than
898 the 1/f background and occur for a minimum number of cycles at a particular frequency. This
899 effectively dissociates narrowband spectral peaks from the arrhythmic background spectrum.
900 Here, we used a one cycle threshold during detection, while defining the power threshold as the
901 95th percentile above the individual background power. A 5-cycle wavelet was used to provide
902 the time-frequency transformations for 49 logarithmically-spaced center frequencies between
903 1 and 64 Hz. Rhythmic episodes were detected as described in [34]. Following the detection of
904 spectral events, the rate of spectral episodes longer than 3 cycles was computed by counting the
905 number of episodes with a mean frequency that fell in a moving window of 3 adjacent center
906 frequencies. This produced a channel-by-frequency representation of spectral event rates,
907 which were the basis for subsequent significance testing. Event rates and statistical results were
908 averaged within frequency bins from 8-12 Hz (alpha) and 14-20 Hz (beta) to assess relations to
909 narrowband entropy and for the visualization of topographies. To visualize the stereotypic
910 depiction of single-trial alpha and beta events, the original time series were time-locked to the
911 trough of individual spectral episodes and averaged across events [c.f., 43]. More specifically,
912 the trough was chosen to be the local minimum during the spectral episode that was closest to
913 the maximum power of the wavelet-transformed signal. To better estimate the local minimum,
914 the signal was low-pass filtered at 25 Hz for alpha and bandpass-filtered between 10 and 25 Hz
915 for beta using a 6th order Butterworth filter. A post-hoc duration threshold of one cycle was
916 used for the visualization of beta events, whereas a three-cycle criterion was used to visualize
917 alpha events. Alpha and beta events were visualized at channels POz and Cz, respectively.

918 **Statistical analyses**

919 Spectral power and entropy were compared across age groups within condition by
920 means of independent samples t-tests; cluster-based permutation tests [94] were performed to
921 control for multiple comparisons. Initially, a clustering algorithm formed clusters based on
922 significant t-tests of individual data points ($p < .05$, two-sided; cluster entry threshold) with the
923 spatial constraint of a cluster covering a minimum of three neighboring channels. Then, the
924 significance of the observed cluster-level statistic, based on the summed t-values within the
925 cluster, was assessed by comparison to the distribution of all permutation-based cluster-level
926 statistics. The final cluster p-value that we report in all Figs was assessed as the proportion of
927 1000 Monte Carlo iterations in which the cluster-level statistic was exceeded. Cluster
928 significance was indicated by p-values below .025 (two-sided cluster significance threshold).
929 Effect sizes for MSE age differences with different filter settings were computed on the basis
930 of the cluster results in the ‘Original’ version. This was also the case for analyses of partial
931 correlations. Raw MSE values were extracted from channels with indicated age differences at
932 the initial three scales 1-3 (>65 Hz) for fine MSE and scales 39-41 (<6.5 Hz) for coarse MSE.
933 R^2 was calculated based on the t-values of an unpaired t-test: $R^2 = \frac{t^2}{t^2 + df}$ [95]. The measure
934 describes the variance in the age difference explained by the measure of interest, with the square
935 root being identical to Pearson’s correlation coefficient between continuous individual values

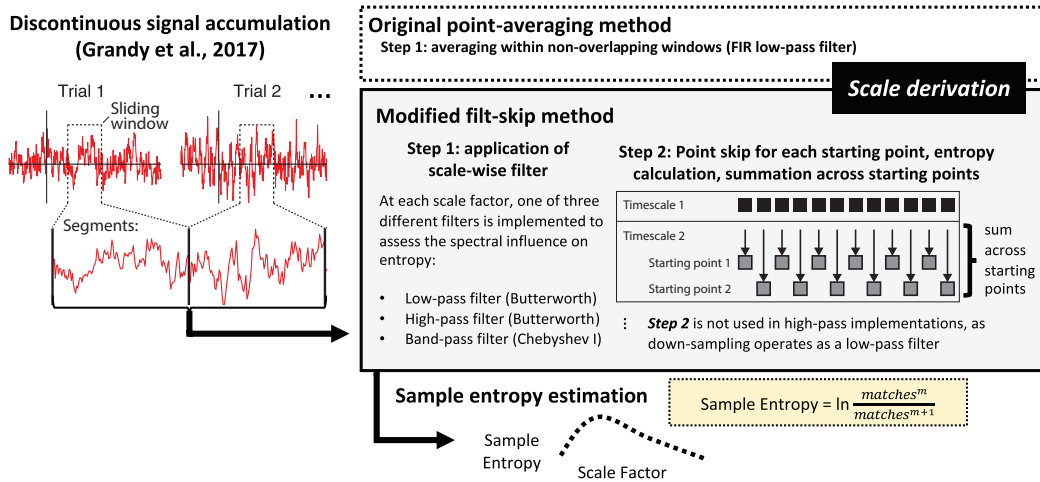
936 and binary age group. Effect sizes were compared using the r-to-z-transform and a successive
 937 comparison of the z-value difference against zero: $Z_{Diff} = \frac{z1-z2}{\sqrt{\frac{1}{N1-3} + \frac{1}{N2-3}}}$ [96]. Unmasked t-
 938 values are presented in support of the assessment of raw statistics in our data [97].

939 Acknowledgements

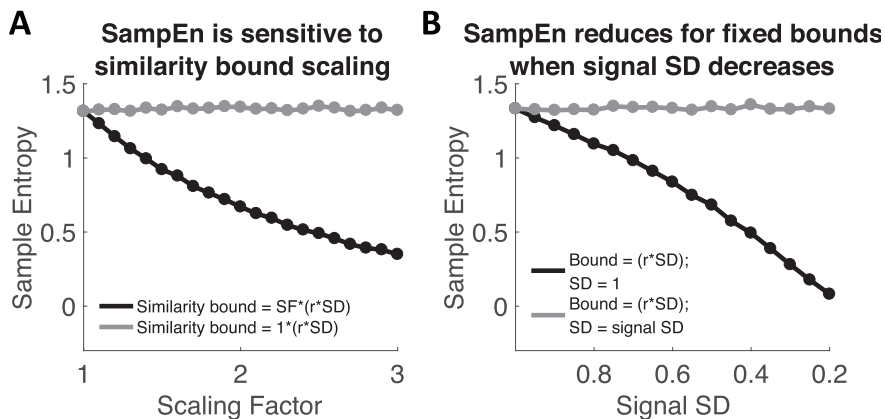
940 We thank our research assistants and participants for their contributions to the present work.

941 Supporting information

942 **S1 File. Systematic literature search assessing the prevalence of global similarity bounds.**

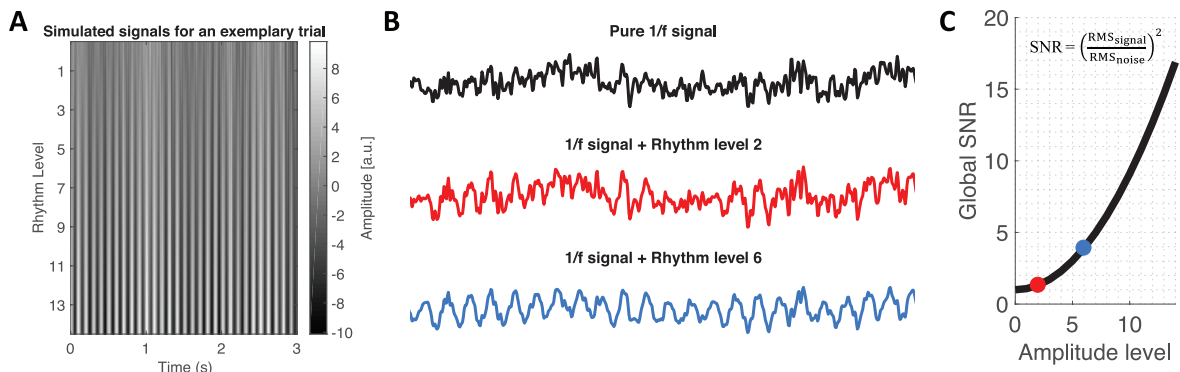


943 **S1 Figure. Overview of modified (mMSE) adaptations.** First, mMSE uses data aggregation across (here:
 944 pseudo-) trials to allow the estimation of coarse scales also from sparse neuroimaging data [90]. These aggregated
 945 signals are then filtered at each scale prior to sample entropy calculation. The ‘Original’ implementation uses
 946 ‘point averaging’ for different scale factors, which is equivalent to a FIR low-pass filter. In adapted applications,
 947 we used a two-step implementation, which we refer to as ‘filt-skip’, which first applies a scale-wise low-, high- or
 948 band-pass filter, and then performs point skipping to down-sample the resulting signals. Finally, the sample
 949 entropy of these signals is similarly assessed using the sample entropy algorithm, which results in multiscale
 950 entropy estimates. Figure adapted with permission from [70].

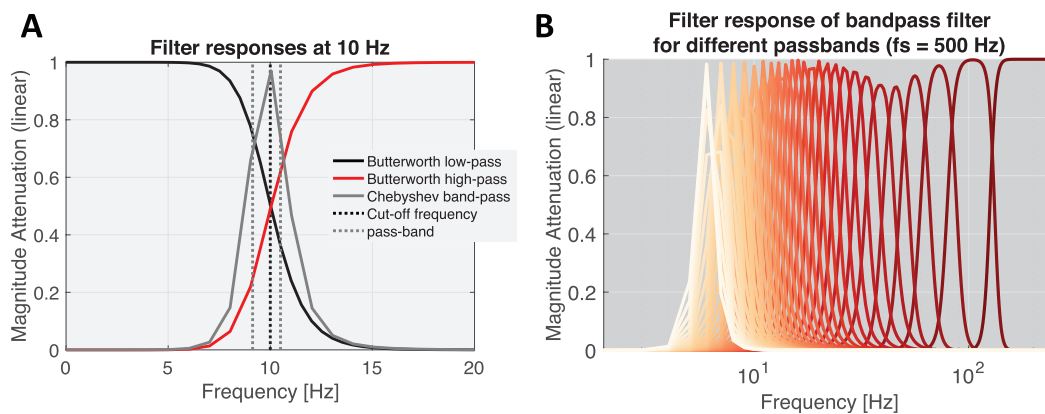


952 **S2 Figure. Liberal similarity bounds reduce sample entropy in simulations.** (A) The plot shows the sample
 953 entropy of simulated white noise signals with constant signal standard deviation (SD) of 1, but varying similarity
 954 bounds. We denote this as a function of a scaling factor (SF) to highlight that such variation may arise from either
 955 variation in r, SD or both. Note that the r parameter is usually fixed and the SD matches the signal SD (gray line),
 956 thus normalizing total signal variance. However, when the similarity bound systematically increases relative to the
 957 signal SD, entropy estimates progressively decrease (black line). (B) A similar scenario applies when fixed and
 958

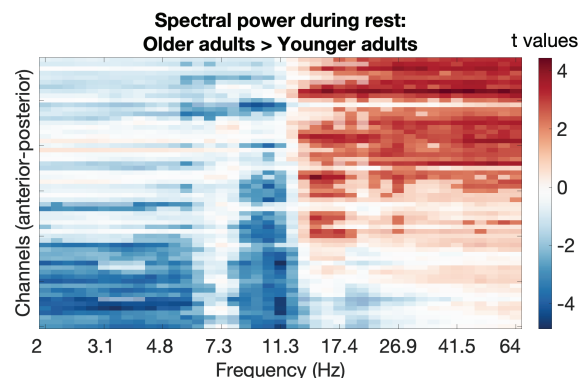
959 large bounds are applied to signals of decreasing variance, as is the case across MSE time scales due to scale-wise
 960 filtering (Fig 2). Whereas no bias is observed when scale-wise signal SD is used for the calculation of similarity
 961 bounds (grey line), entropy estimates systematically decrease when the SD of the original signal are used (black
 962 line). Hence, the mismatched similarity bounds introduced entropy decreases although no changes to the structure
 963 of the (here white noise) signals were introduced.



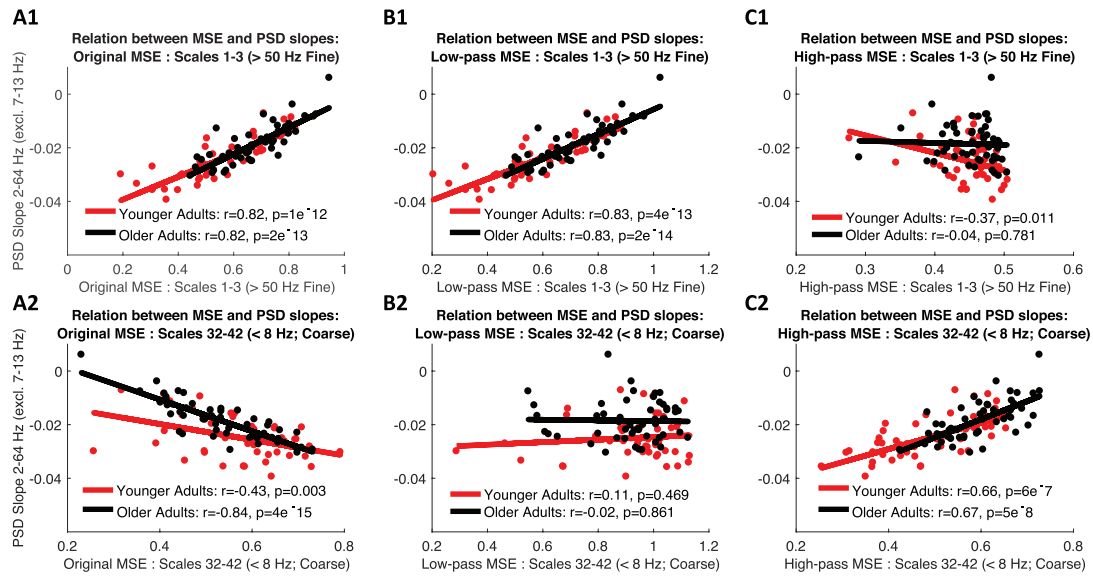
964 **S3 Figure. Examples of simulated rhythmicity projected into pink noise.** (A) Top-down view of time-series
 965 from an exemplary simulated trial for a pure 1/f signal pink noise signal and at different magnitudes of added alpha
 966 rhythmicity. (B) Exemplary time series in 2D view. The red time series indicates an example time series for the
 967 level of rhythmicity shown in Fig 5. (C) Simulated SNR as a function of amplitude level. The dots indicate SNR
 968 for the levels depicted in panel B.
 969



970 **S4 Figure. Filter magnitude responses.** (A) Filter magnitude responses at 10 Hz. Note that magnitude responses
 971 have been squared due to two-pass filtering to achieve zero-phase offsets. (B) Filter magnitudes of Bandpass filters
 972 (3rd order type I Chebyshev filter with 1dB passband ripple) at different time scales (red-to-orange indicating fine-
 973 to-coarse time scales). Note that only a high-pass filter (6th order Butterworth filter) is applied at the first scale.
 974



975 **S5 Figure. T-values for age group differences in spectral power (OA > YA).** Statistical significance ($p < .05$)
 976 was assessed by means of cluster-based permutation tests and is indicated via opacity.
 977



978
979
980
981
982
983
984

S6 Figure. Methods- and scale-dependent associations between sample entropy and PSD slopes. ‘Original’ settings indicate a strong positive association at fine scales (A1) that turns negative at coarse scales (A2), likely due to coarse-scale biases by the scale-invariant similarity criterion. In line with this notion, scale-wise adaptation of thresholds retains the fine-scale effect (B1), while abolishing the coarse-scale inversion (B2). Crucially, the entropy of exclusively high-frequency signals does not positively relate to PSD slopes (C1), whereas the association reemerges once slow fluctuations are added into the signal (C2).

985 **Additional Information**

986 **Data availability**

987 Raw empirical data is provided at <https://osf.io/q3vxm/>. Code used to produce simulations,
988 empirical analyses and figures is provided at https://git.mpib-berlin.mpg.de/LNDG/rhythms_entropy. The code implementing the mMSE algorithm is
989 available from <https://github.com/LNDG/mMSE>.
990

991 **Funding**

992 This study was conducted within the ‘Lifespan Neural Dynamics Group’ within the Max
993 Planck UCL Centre for Computational Psychiatry and Ageing Research in the Max Planck
994 Institute for Human Development (MPIB) in Berlin, Germany. DDG and NAK were supported
995 by an Emmy Noether Programme grant (to DDG) from the German Research Foundation, and
996 by the Max Planck UCL Centre for Computational Psychiatry and Ageing Research. JQK is a
997 pre-doctoral fellow supported by the International Max Planck Research School on
998 Computational Methods in Psychiatry and Ageing Research (IMPRS COMP2PSYCH). The
999 participating institutions are the Max Planck Institute for Human Development, Berlin,
1000 Germany, and University College London, London, UK. For more information, see
1001 <https://www.mps-ucl-centre.mpg.de/en/comp2psych>.

1002 **Competing interests**

1003 The authors declare that there are no conflicts of interest.

1004 **Author contributions**

1005 Conceptualization – JQK, DDG, NAK
1006 Data Curation – JQK, NAK
1007 Formal Analysis – JQK
1008 Funding Acquisition – DDG
1009 Investigation – JQK, NAK, DDG
1010 Methodology – JQK, NAK, DDG
1011 Project Administration – JQK, DDG
1012 Resources – NAK, DDG
1013 Software – JQK, NAK
1014 Supervision - DDG
1015 Validation – JQK
1016 Visualization – JQK
1017 Writing – Original Draft Preparation – JQK
1018 Writing – Review & Editing – JQK, NAK, DDG

1019 **References**

- 1020 1. Buzsaki G, Draguhn A. Neuronal oscillations in cortical networks. *Science*.
1021 2004;304(5679):1926-9. doi: 10.1126/science.1099745. PubMed PMID:
1022 WOS:000222241600031.
- 1023 2. Wang XJ. Neurophysiological and computational principles of cortical rhythms in
1024 cognition. *Physiol Rev*. 2010;90(3):1195-268. Epub 2010/07/29. doi:
1025 10.1152/physrev.00035.2008. PubMed PMID: 20664082; PubMed Central PMCID:
1026 PMCPMC2923921.
- 1027 3. Breakspear M. Dynamic models of large-scale brain activity. *Nat Neurosci*.
1028 2017;20(3):340-52. doi: 10.1038/nn.4497. PubMed PMID: WOS:000394920400007.
- 1029 4. Vakorin VA, McIntosh AR. Mapping the Multiscale Information Content of Complex
1030 Brain Signals. *Comput Neurosci-Mit*. 2012:183-208. PubMed PMID:
1031 WOS:000315291000011.
- 1032 5. Stam CJ. Nonlinear dynamical analysis of EEG and MEG: review of an emerging
1033 field. *Clin Neurophysiol*. 2005;116(10):2266-301. Epub 2005/08/24. doi:
1034 10.1016/j.clinph.2005.06.011. PubMed PMID: 16115797.
- 1035 6. Garrett DD, Samanez-Larkin GR, MacDonald SW, Lindenberger U, McIntosh AR,
1036 Grady CL. Moment-to-moment brain signal variability: a next frontier in human brain
1037 mapping? *Neurosci Biobehav Rev*. 2013;37(4):610-24. Epub 2013/03/06. doi:
1038 10.1016/j.neubiorev.2013.02.015. PubMed PMID: 23458776; PubMed Central
1039 PMCID: PMCPMC3732213.
- 1040 7. Costa M, Goldberger AL, Peng CK. Multiscale entropy analysis of complex
1041 physiologic time series. *Phys Rev Lett*. 2002;89(6). doi:
1042 10.1103/PhysRevLett.89.068102. PubMed PMID: WOS:000177009600047.
- 1043 8. Costa M, Goldberger AL, Peng CK. Multiscale entropy analysis of biological signals.
1044 *Phys Rev E*. 2005;71(2). doi: 10.1103/PhysRevE.71.021906. PubMed PMID:
1045 WOS:000228245700047.
- 1046 9. Richman JS, Moorman JR. Physiological time-series analysis using approximate
1047 entropy and sample entropy. *Am J Physiol-Heart C*. 2000;278(6):H2039-H49.
1048 PubMed PMID: WOS:000087573500038.
- 1049 10. Bruce EN, Bruce MC, Vennelaganti S. Sample Entropy Tracks Changes in
1050 Electroencephalogram Power Spectrum With Sleep State and Aging. *J Clin*
1051 *Neurophysiol*. 2009;26(4):257-66. doi: 10.1097/WNP.0b013e3181b2f1e3. PubMed
1052 PMID: WOS:000268746000007.
- 1053 11. Jaworska N, Wang HY, Smith DM, Blier P, Knott V, Protzner AB. Pre-treatment EEG
1054 signal variability is associated with treatment success in depression. *Neuroimage-Clin*.
1055 2018;17:368-77. doi: 10.1016/j.nicl.2017.10.035. PubMed PMID:
1056 WOS:000426180300040.
- 1057 12. McIntosh AR, Vakorin V, Kovacevic N, Wang H, Diaconescu A, Protzner AB.
1058 Spatiotemporal Dependency of Age-Related Changes in Brain Signal Variability.
1059 *Cereb Cortex*. 2014;24(7):1806-17. doi: 10.1093/cercor/bht030. PubMed PMID:
1060 WOS:000338110900010.
- 1061 13. Miskovic V, MacDonald KJ, Rhodes LJ, Cote KA. Changes in EEG multiscale
1062 entropy and power-law frequency scaling during the human sleep cycle. *Hum Brain*

- 1063 Mapp. 2019;40(2):538-51. doi: 10.1002/hbm.24393. PubMed PMID:
1064 WOS:000460481300014.
- 1065 14. Wang H, McIntosh AR, Kovacevic N, Karachalios M, Protzner AB. Age-related
1066 Multiscale Changes in Brain Signal Variability in Pre-task versus Post-task Resting-
1067 state EEG. *J Cogn Neurosci*. 2016;28(7):971-84. Epub 2016/03/05. doi:
1068 10.1162/jocn_a_00947. PubMed PMID: 26942319.
- 1069 15. Sleimen-Malkoun R, Perdikis D, Muller V, Blanc JL, Huys R, Temprado JJ, et al.
1070 Brain Dynamics of Aging: Multiscale Variability of EEG Signals at Rest and during
1071 an Auditory Oddball Task(1,2,3). *Eneuro*. 2015;2(3). doi: 10.1523/ENEURO.0067-
1072 14.2015. PubMed PMID: WOS:000218581400012.
- 1073 16. Werkle-Bergner M, Grandy TH, Chicherio C, Schmiedek F, Lovden M, Lindenberger
1074 U. Coordinated within-Trial Dynamics of Low-Frequency Neural Rhythms Controls
1075 Evidence Accumulation. *J Neurosci*. 2014;34(25):8519-28. doi:
1076 10.1523/Jneurosci.3801-13.2014. PubMed PMID: WOS:000338449200014.
- 1077 17. Yang AC, Wang SJ, Lai KL, Tsai CF, Yang CH, Hwang JP, et al. Cognitive and
1078 neuropsychiatric correlates of EEG dynamic complexity in patients with Alzheimer's
1079 disease. *Prog Neuro-Psychoph*. 2013;47:52-61. doi: 10.1016/j.pnpbp.2013.07.022.
1080 PubMed PMID: WOS:000326682300009.
- 1081 18. Takahashi T, Cho RY, Mizuno T, Kikuchi M, Murata T, Takahashi K, et al.
1082 Antipsychotics reverse abnormal EEG complexity in drug-naive schizophrenia: A
1083 multiscale entropy analysis. *Neuroimage*. 2010;51(1):173-82. doi:
1084 10.1016/j.neuroimage.2010.02.009. PubMed PMID: WOS:000276480200018.
- 1085 19. Mejias JF, Murray JD, Kennedy H, Wang XJ. Feedforward and feedback frequency-
1086 dependent interactions in a large-scale laminar network of the primate cortex. *Sci Adv*.
1087 2016;2(11). doi: 10.1126/sciadv.1601335. PubMed PMID: WOS:000391267800032.
- 1088 20. Buzsaki G, Logothetis N, Singer W. Scaling Brain Size, Keeping Timing:
1089 Evolutionary Preservation of Brain Rhythms. *Neuron*. 2013;80(3):751-64. doi:
1090 10.1016/j.neuron.2013.10.002. PubMed PMID: WOS:000326609900019.
- 1091 21. von Stein A, Sarnthein J. Different frequencies for different scales of cortical
1092 integration: from local gamma to long range alpha/theta synchronization. *Int J*
1093 *Psychophysiol*. 2000;38(3):301-13. doi: 10.1016/S0167-8760(00)00172-0. PubMed
1094 PMID: WOS:000165915000009.
- 1095 22. Fries P. Neuronal Gamma-Band Synchronization as a Fundamental Process in Cortical
1096 Computation. *Annu Rev Neurosci*. 2009;32:209-24. doi:
1097 10.1146/annurev.neuro.051508.135603. PubMed PMID: WOS:000268504100009.
- 1098 23. Courtiol J, Perdikis D, Petkoski S, Muller V, Huys R, Sleimen-Malkoun R, et al. The
1099 multiscale entropy: Guidelines for use and interpretation in brain signal analysis. *J*
1100 *Neurosci Meth*. 2016;273:175-90. doi: 10.1016/j.jneumeth.2016.09.004. PubMed
1101 PMID: WOS:000387195800017.
- 1102 24. Costa M, Goldberger AL, Peng CK. Comment on "Multiscale entropy analysis of
1103 complex physiologic time series" - Reply. *Phys Rev Lett*. 2004;92(8). doi:
1104 10.1103/PhysRevLett.92.089804. PubMed PMID: WOS:000189266100069.
- 1105 25. Nikulin VV, Brismar T. Comment on "Multiscale entropy analysis of complex
1106 physiologic time series". *Phys Rev Lett*. 2004;92(8). doi:
1107 10.1103/PhysRevLett.92.089803. PubMed PMID: WOS:000189266100068.

- 1108 26. Shafiei G, Zeighami Y, Clark CA, Coull JT, Nagano-Saito A, Leyton M, et al.
1109 Dopamine Signaling Modulates the Stability and Integration of Intrinsic Brain
1110 Networks. *Cereb Cortex*. 2019;29(1):397-409. doi: 10.1093/cercor/bhy264. PubMed
1111 PMID: WOS:000459518500030.
- 1112 27. Azami H, Escudero J. Coarse-Graining Approaches in Univariate Multiscale Sample
1113 and Dispersion Entropy. *Entropy*. 2018;20(2). doi: 10.3390/e20020138. PubMed
1114 PMID: WOS:000426793900061.
- 1115 28. Miskovic V, Owens M, Kuntzelman K, Gibb BE. Charting moment-to-moment brain
1116 signal variability from early to late childhood. *Cortex*. 2016;83:51-61. Epub
1117 2016/08/02. doi: 10.1016/j.cortex.2016.07.006. PubMed PMID: 27479615; PubMed
1118 Central PMCID: PMC5042835.
- 1119 29. Valencia JF, Porta A, Vallverdu M, Claria F, Baranowski R, Orłowska-Baranowska E,
1120 et al. Refined Multiscale Entropy: Application to 24-h Holter Recordings of Heart
1121 Period Variability in Healthy and Aortic Stenosis Subjects. *Ieee T Bio-Med Eng*.
1122 2009;56(9):2202-13. doi: 10.1109/Tbme.2009.2021986. PubMed PMID:
1123 WOS:000269154100008.
- 1124 30. Buzsaki G, Mizuseki K. The log-dynamic brain: how skewed distributions affect
1125 network operations. *Nat Rev Neurosci*. 2014;15(4):264-78. doi: 10.1038/nrn3687.
1126 PubMed PMID: WOS:000333256600012.
- 1127 31. He BYJ. Scale-free brain activity: past, present, and future. *Trends Cogn Sci*.
1128 2014;18(9):480-7. doi: 10.1016/j.tics.2014.04.003. PubMed PMID:
1129 WOS:000341613000010.
- 1130 32. Waschke L, Wostmann M, Obleser J. States and traits of neural irregularity in the age-
1131 varying human brain. *Sci Rep-Uk*. 2017;7. doi: 10.1038/s41598-017-17766-4.
1132 PubMed PMID: WOS:000417689400005.
- 1133 33. Haller M, Donoghue T, Peterson E, Varma P, Sebastian P, Gao R, et al.
1134 Parameterizing neural power spectra. *bioRxiv*. 2018.
- 1135 34. Kosciessa JQ, Grandy TH, Garrett DD, Werkle-Bergner M. Single-trial
1136 characterization of neural rhythms: Potential and challenges. *Neuroimage*.
1137 2019;116331. doi: <https://doi.org/10.1016/j.neuroimage.2019.116331>.
- 1138 35. Lopes da Silva F. EEG and MEG: relevance to neuroscience. *Neuron*.
1139 2013;80(5):1112-28. Epub 2013/12/10. doi: 10.1016/j.neuron.2013.10.017. PubMed
1140 PMID: 24314724.
- 1141 36. Park JH, Kim S, Kim CH, Cichocki A, Kim K. Multiscale entropy analysis of EEG
1142 from patients under different pathological conditions. *Fractals*. 2007;15(4):399-404.
1143 doi: 10.1142/S0218348x07003691. PubMed PMID: WOS:000252021600010.
- 1144 37. McIntosh AR. *Neurocognitive Aging and Brain Signal Complexity*. Oxford University
1145 Press; 2019.
- 1146 38. McIntosh AR, Kovacevic N, Itier RJ. Increased Brain Signal Variability Accompanies
1147 Lower Behavioral Variability in Development. *Plos Comput Biol*. 2008;4(7). doi:
1148 10.1371/journal.pcbi.1000106. PubMed PMID: WOS:000260039300027.
- 1149 39. Leirer VM, Wienbruch C, Kolassa S, Schlee W, Elbert T, Kolassa IT. Changes in
1150 cortical slow wave activity in healthy aging. *Brain Imaging Behav*. 2011;5(3):222-8.
1151 doi: 10.1007/s11682-011-9126-3. PubMed PMID: WOS:000293498500007.

- 1152 40. Vlahou EL, Thurm F, Kolassa IT, Schlee W. Resting-state slow wave power, healthy
1153 aging and cognitive performance. *Sci Rep-Uk*. 2014;4. doi: 10.1038/srep05101.
1154 PubMed PMID: WOS:000336516800002.
- 1155 41. Voytek B, Kramer MA, Case J, Lepage KQ, Tempesta ZR, Knight RT, et al. Age-
1156 Related Changes in 1/f Neural Electrophysiological Noise. *J Neurosci*.
1157 2015;35(38):13257-65. doi: 10.1523/Jneurosci.2332-14.2015. PubMed PMID:
1158 WOS:000363660200027.
- 1159 42. Hipp JF, Siegel M. Dissociating neuronal gamma-band activity from cranial and
1160 ocular muscle activity in EEG. *Front Hum Neurosci*. 2013;7. doi:
1161 10.3389/fnhum.2013.00338. PubMed PMID: WOS:000321588600001.
- 1162 43. Sherman MA, Lee S, Law R, Haegens S, Thorn CA, Hamalainen MS, et al. Neural
1163 mechanisms of transient neocortical beta rhythms: Converging evidence from humans,
1164 computational modeling, monkeys, and mice. *P Natl Acad Sci USA*.
1165 2016;113(33):E4885-E94. doi: 10.1073/pnas.1604135113. PubMed PMID:
1166 WOS:000381399200018.
- 1167 44. Shin H, Law R, Tsutsui S, Moore CI, Jones SR. The rate of transient beta frequency
1168 events predicts behavior across tasks and species. *Elife*. 2017;6. doi:
1169 10.7554/eLife.29086. PubMed PMID: WOS:000414984800001.
- 1170 45. Waschke L, Tune S, Obleser J. Local cortical desynchronization and pupil-linked
1171 arousal differentially shape brain states for optimal sensory performance. *Elife*.
1172 2019;8. Epub 2019/12/11. doi: 10.7554/eLife.51501. PubMed PMID: 31820732.
- 1173 46. Contreras D, Steriade M. Synchronization of low-frequency rhythms in
1174 corticothalamic networks. *Neuroscience*. 1997;76(1):11-24. PubMed PMID:
1175 WOS:A1997VY25600003.
- 1176 47. Harris KD, Thiele A. Cortical state and attention. *Nat Rev Neurosci*. 2011;12(9):509-
1177 23. doi: 10.1038/nrn3084. PubMed PMID: WOS:000294049200013.
- 1178 48. Marguet SL, Harris KD. State-Dependent Representation of Amplitude-Modulated
1179 Noise Stimuli in Rat Auditory Cortex. *J Neurosci*. 2011;31(17):6414-20. doi:
1180 10.1523/Jneurosci.5773-10.2011. PubMed PMID: WOS:000289934600018.
- 1181 49. Gao R, Peterson EJ, Voytek B. Inferring synaptic excitation/inhibition balance from
1182 field potentials. *Neuroimage*. 2017;158:70-8. doi: 10.1016/j.neuroimage.2017.06.078.
1183 PubMed PMID: WOS:000411450600008.
- 1184 50. Peterson EJ, Rosen BQ, Campbell AM, Belger A, Voytek B. 1/f neural noise is a
1185 better predictor of schizophrenia than neural oscillations. *bioRxiv*. 2018.
- 1186 51. Sheehan TC, Sreekumar V, Inati SK, Zaghoul KA. Signal Complexity of Human
1187 Intracranial EEG Tracks Successful Associative-Memory Formation across
1188 Individuals. *J Neurosci*. 2018;38(7):1744-55. doi: 10.1523/Jneurosci.2389-17.2017.
1189 PubMed PMID: WOS:000424987700012.
- 1190 52. Kaffashi F, Foglyano R, Wilson CG, Loparo KA. The effect of time delay on
1191 Approximate & Sample Entropy calculations. *Physica D*. 2008;237(23):3069-74. doi:
1192 10.1016/j.physd.2008.06.005. PubMed PMID: WOS:000261463000010.
- 1193 53. Misic B, Vakorin VA, Paus T, McIntosh AR. Functional embedding predicts the
1194 variability of neural activity. *Front Syst Neurosci*. 2011;5:90. Epub 2011/12/14. doi:
1195 10.3389/fnsys.2011.00090. PubMed PMID: 22164135; PubMed Central PMCID:
1196 PMCPMC3225043.

- 1197 54. Deco G, Jirsa VK, McIntosh AR. Resting brains never rest: computational insights
1198 into potential cognitive architectures. *Trends Neurosci.* 2013;36(5):268-74. Epub
1199 2013/04/09. doi: 10.1016/j.tins.2013.03.001. PubMed PMID: 23561718.
- 1200 55. Deco G, Jirsa VK, McIntosh AR. Emerging concepts for the dynamical organization
1201 of resting-state activity in the brain. *Nat Rev Neurosci.* 2011;12(1):43-56. Epub
1202 2010/12/21. doi: 10.1038/nrn2961. PubMed PMID: 21170073.
- 1203 56. Ishii R, Canuet L, Aoki Y, Hata M, Iwase M, Ikeda S, et al. Healthy and Pathological
1204 Brain Aging: From the Perspective of Oscillations, Functional Connectivity, and
1205 Signal Complexity. *Neuropsychobiology.* 2017;75(4):151-61. Epub 2018/02/22. doi:
1206 10.1159/000486870. PubMed PMID: 29466802.
- 1207 57. Caplan JB, Bottomley M, Kang P, Dixon RA. Distinguishing rhythmic from non-
1208 rhythmic brain activity during rest in healthy neurocognitive aging. *Neuroimage.*
1209 2015;112:341-52. Epub 2015/03/15. doi: 10.1016/j.neuroimage.2015.03.001. PubMed
1210 PMID: 25769279; PubMed Central PMCID: PMC4408255.
- 1211 58. Rossiter HE, Davis EM, Clark EV, Boudrias MH, Ward NS. Beta oscillations reflect
1212 changes in motor cortex inhibition in healthy ageing. *Neuroimage.* 2014;91:360-5.
1213 Epub 2014/01/21. doi: 10.1016/j.neuroimage.2014.01.012. PubMed PMID: 24440529;
1214 PubMed Central PMCID: PMC3988925.
- 1215 59. Cole S, Voytek B. Cycle-by-cycle analysis of neural oscillations. *bioRxiv.* 2018.
- 1216 60. Heisz JJ, Shedden JM, McIntosh AR. Relating brain signal variability to knowledge
1217 representation. *Neuroimage.* 2012;63(3):1384-92. doi:
1218 10.1016/j.neuroimage.2012.08.018. PubMed PMID: WOS:000310379100040.
- 1219 61. Lippe S, Kovacevic N, McIntosh AR. Differential maturation of brain signal
1220 complexity in the human auditory and visual system. *Front Hum Neurosci.* 2009;3.
1221 doi: 10.3389/neuro.09.048.2009. PubMed PMID: WOS:000274619300008.
- 1222 62. Mizuno T, Takahashi T, Cho RY, Kikuchi M, Murata T, Takahashi K, et al.
1223 Assessment of EEG dynamical complexity in Alzheimer's disease using multiscale
1224 entropy. *Clin Neurophysiol.* 2010;121(9):1438-46. doi: 10.1016/j.clinph.2010.03.025.
1225 PubMed PMID: WOS:000280555400007.
- 1226 63. Szostakiwskyj JMH, Willatt SE, Cortese F, Protzner AB. The modulation of EEG
1227 variability between internally-and externally-driven cognitive states varies with
1228 maturation and task performance. *Plos One.* 2017;12(7). doi:
1229 10.1371/journal.pone.0181894. PubMed PMID: WOS:000406575700098.
- 1230 64. Takahashi T, Cho RY, Murata T, Mizuno T, Kikuchi M, Mizukami K, et al. Age-
1231 related variation in EEG complexity to photic stimulation: A multiscale entropy
1232 analysis. *Clin Neurophysiol.* 2009;120(3):476-83. doi: 10.1016/j.clinph.2008.12.043.
1233 PubMed PMID: WOS:000265772400006.
- 1234 65. Carpentier SM, McCulloch AR, Brown TM, Ritter P, Wang Z, Salimpoor V, et al.
1235 Complexity matching: brain signals mirror environment information patterns during
1236 music listening and reward. *bioRxiv.* 2019.
- 1237 66. Raja Beharelle A, Kovacevic N, McIntosh AR, Levine B. Brain signal variability
1238 relates to stability of behavior after recovery from diffuse brain injury. *Neuroimage.*
1239 2012;60(2):1528-37. Epub 2012/01/21. doi: 10.1016/j.neuroimage.2012.01.037.
1240 PubMed PMID: 22261371; PubMed Central PMCID: PMC3303989.

- 1241 67. Catarino A, Churches O, Baron-Cohen S, Andrade A, Ring H. Atypical EEG
1242 complexity in autism spectrum conditions: A multiscale entropy analysis. *Clin*
1243 *Neurophysiol.* 2011;122(12):2375-83. doi: 10.1016/j.clinph.2011.05.004. PubMed
1244 PMID: WOS:000296583000008.
- 1245 68. Masic B, Doesburg SM, Fatima Z, Vidal J, Vakorin VA, Taylor MJ, et al. Coordinated
1246 Information Generation and Mental Flexibility: Large-Scale Network Disruption in
1247 Children with Autism. *Cereb Cortex.* 2015;25(9):2815-27. doi:
1248 10.1093/cercor/bhu082. PubMed PMID: WOS:000361464000042.
- 1249 69. Ueno K, Takahashi T, Takahashi K, Mizukami K, Tanaka Y, Wada Y.
1250 Neurophysiological basis of creativity in healthy elderly people: A multiscale entropy
1251 approach. *Clin Neurophysiol.* 2015;126(3):524-31. doi: 10.1016/j.clinph.2014.06.032.
1252 PubMed PMID: WOS:000349616700015.
- 1253 70. Kloosterman NA, Kosciessa JQ, Lindenberger U, Fahrenfort JJ, Garrett DD. Boosting
1254 Brain Signal Variability Underlies Liberal Shifts in Decision Bias. *bioRxiv.* 2019.
- 1255 71. Theiler J, Eubank S, Longtin A, Galdrikian B, Farmer JD. Testing for Nonlinearity in
1256 Time-Series - the Method of Surrogate Data. *Physica D.* 1992;58(1-4):77-94. doi:
1257 10.1016/0167-2789(92)90102-S. PubMed PMID: WOS:A1992JV85800006.
- 1258 72. Garrett DD, Grandy TH, Werkle-Bergner M. The neural forest and the trees: On
1259 distinguishing the variance of a brain signal from its information content. *Annual*
1260 *Alpine Brain Imaging Meeting; Champéry, Switzerland2014.*
- 1261 73. Grandy TH, Garrett DD, Lindenberger U, Werkle-Bergner M. Exploring the limits of
1262 complexity measures for the analysis of age differences in neural signals. *Dallas*
1263 *Aging and Cognition Conference; Dallas, TX, USA2013.*
- 1264 74. Takens F. Detecting Nonlinearities in Stationary Time Series. *Int J Bifurcat Chaos.*
1265 1993;3(2):241-56. doi: 10.1142/S0218127493000192. PubMed PMID:
1266 WOS:000209750900002.
- 1267 75. Kloosterman NA, de Gee JW, Werkle-Bergner M, Lindenberger U, Garrett DD,
1268 Fahrenfort JJ. Humans strategically shift decision bias by flexibly adjusting sensory
1269 evidence accumulation. *Elife.* 2019;8. Epub 2019/02/07. doi: 10.7554/eLife.37321.
1270 PubMed PMID: 30724733; PubMed Central PMCID: PMC6365056.
- 1271 76. Simpraga S, Alvarez-Jimenez R, Mansvelder HD, van Gerven JMA, Groeneveld GJ,
1272 Poil SS, et al. EEG machine learning for accurate detection of cholinergic intervention
1273 and Alzheimer's disease. *Sci Rep-Uk.* 2017;7. doi: 10.1038/s41598-017-06165-4.
1274 PubMed PMID: WOS:000405746500086.
- 1275 77. Stoyanov M, Gunzburger M, Burkardt J. Pink noise, $1/f$ (alpha) noise, and their effect
1276 on solutions of differential equations. *Int J Uncertain Quan.* 2011;1(3):257-78. doi:
1277 10.1615/Int.J.UncertaintyQuantification.2011003089. PubMed PMID:
1278 WOS:000209100100005.
- 1279 78. Oldfield RC. The Assessment and Analysis of Handedness: The Edinburgh Inventory.
1280 *Neuropsychologia.* 1971;9(1):97-113. doi: 10.1016/0028-3932(71)90067-4. PubMed
1281 PMID: WOS:A1971J199600013.
- 1282 79. Folstein MF, Robins LN, Helzer JE. The Mini-Mental State Examination. *Arch Gen*
1283 *Psychiat.* 1983;40(7):812-. PubMed PMID: WOS:A1983QX57000014.
- 1284 80. Kessler J, Markowitsch H, Denzler P. Mini-mental-status-test (MMST). Göttingen:
1285 Beltz Test GMBH; 2000.

- 1286 81. Oostenveld R, Praamstra P. The five percent electrode system for high-resolution EEG
1287 and ERP measurements. *Clin Neurophysiol.* 2001;112(4):713-9. doi: 10.1016/S1388-
1288 2457(00)00527-7. PubMed PMID: WOS:000168113100018.
- 1289 82. Oostenveld R, Fries P, Maris E, Schoffelen JM. FieldTrip: Open Source Software for
1290 Advanced Analysis of MEG, EEG, and Invasive Electrophysiological Data. *Comput*
1291 *Intel Neurosc.* 2011. doi: 10.1155/2011/156869. PubMed PMID:
1292 WOS:000208906100004.
- 1293 83. Bell AJ, Sejnowski TJ. An Information Maximization Approach to Blind Separation
1294 and Blind Deconvolution. *Neural Comput.* 1995;7(6):1129-59. doi:
1295 10.1162/neco.1995.7.6.1129. PubMed PMID: WOS:A1995RZ70200001.
- 1296 84. Nolan H, Whelan R, Reilly RB. FASTER: Fully Automated Statistical Thresholding
1297 for EEG artifact Rejection. *J Neurosci Meth.* 2010;192(1):152-62. doi:
1298 10.1016/j.jneumeth.2010.07.015. PubMed PMID: WOS:000283477500020.
- 1299 85. Perrin F, Pernier J, Bertrand O, Echallier JF. Spherical Splines for Scalp Potential and
1300 Current-Density Mapping. *Electroen Clin Neuro.* 1989;72(2):184-7. doi:
1301 10.1016/0013-4694(89)90180-6. PubMed PMID: WOS:A1989T157400011.
- 1302 86. Heisz JJ, McIntosh AR. Applications of EEG Neuroimaging Data: Event-related
1303 Potentials, Spectral Power, and Multiscale Entropy. *Jove-Journal of Visualized*
1304 *Experiments.* 2013;(76). doi: 10.3791/50131. PubMed PMID:
1305 WOS:000209227800013.
- 1306 87. Semmlow JL. *Biosignal and medical image processing*: CRC press; 2008.
- 1307 88. Widmann A, Schroger E, Maess B. Digital filter design for electrophysiological data -
1308 a practical approach. *J Neurosci Meth.* 2015;250:34-46. doi:
1309 10.1016/j.jneumeth.2014.08.002. PubMed PMID: WOS:000356978900005.
- 1310 89. Wu SD, Wu CW, Lin SG, Lee KY, Peng CK. Analysis of complex time series using
1311 refined composite multiscale entropy. *Phys Lett A.* 2014;378(20):1369-74. doi:
1312 10.1016/j.physleta.2014.03.034. PubMed PMID: WOS:000335704900007.
- 1313 90. Grandy TH, Garrett DD, Schmiedek F, Werkle-Bergner M. On the estimation of brain
1314 signal entropy from sparse neuroimaging data. *Sci Rep-Uk.* 2016;6. doi:
1315 10.1038/srep23073. PubMed PMID: WOS:000372915300001.
- 1316 91. Jones SR. When brain rhythms aren't 'rhythmic': implication for their mechanisms and
1317 meaning. *Curr Opin Neurobiol.* 2016;40:72-80. doi: 10.1016/j.conb.2016.06.010.
1318 PubMed PMID: WOS:000386405800012.
- 1319 92. Caplan JB, Madsen JR, Raghavachari S, Kahana MJ. Distinct patterns of brain
1320 oscillations underlie two basic parameters of human maze learning. *J Neurophysiol.*
1321 2001;86(1):368-80. PubMed PMID: WOS:000169955100033.
- 1322 93. Whitten TA, Hughes AM, Dickson CT, Caplan JB. A better oscillation detection
1323 method robustly extracts EEG rhythms across brain state changes: The human alpha
1324 rhythm as a test case. *Neuroimage.* 2011;54(2):860-74. doi:
1325 10.1016/j.neuroimage.2010.08.064. PubMed PMID: WOS:000285486000013.
- 1326 94. Maris E, Oostenveld R. Nonparametric statistical testing of EEG- and MEG-data. *J*
1327 *Neurosci Meth.* 2007;164(1):177-90. doi: 10.1016/j.jneumeth.2007.03.024. PubMed
1328 PMID: WOS:000248170300019.

- 1329 95. Lakens D. Calculating and reporting effect sizes to facilitate cumulative science: a
1330 practical primer for t-tests and ANOVAs. *Front Psychol.* 2013;4. doi:
1331 10.3389/fpsyg.2013.00863. PubMed PMID: WOS:000331576200001.
- 1332 96. Brandner FA. A test of the significance of the difference of the correlation coefficients
1333 in normal bivariate samples. *Biometrika.* 1933;25:102-9. doi: 10.1093/biomet/25.1-
1334 2.102. PubMed PMID: WOS:000200863000008.
- 1335 97. Allen EA, Erhardt EB, Calhoun VD. Data Visualization in the Neurosciences:
1336 Overcoming the Curse of Dimensionality. *Neuron.* 2012;74(4):603-8. doi:
1337 10.1016/j.neuron.2012.05.001. PubMed PMID: WOS:000304747200004.
1338

Supplementary Information for

Standard multiscale entropy reflects spectral power at mismatched temporal scales

Julian Q. Kosciessa, Niels A. Kloosterman, and Douglas D. Garrett

Email: kosciessa@mpib-berlin.mpg.de; garrett@mpib-berlin.mpg.de

S1 Text. Systematic literature search assessing the prevalence of global similarity bounds. We performed a systematic literature search to assess the prevalence of global similarity bounds in current neuroscientific applications (heart rate variability applications are specifically marked). We searched Pubmed (<https://www.ncbi.nlm.nih.gov/pubmed>) with the following terms: *(MSE AND sample entropy AND EEG) OR (MSE AND brain AND variability) OR (MSE AND EEG AND variability) OR (multiscale entropy AND EEG AND variability)*. We excluded any studies that did not assess multiscale entropy, including studies that were restricted to sample entropy at scale 1. In addition, we added references from the main text that were not captured by the systematic search (highlighted in grey). For MSE applications, we checked the text for a notion of how similarity bounds were computed, i.e., whether it was calculated as $r \times SD$ of the original time series or the coarse-grained time series. The following sections list the results of this qualitative review and is purely intended to characterize the prevalence of global similarity bounds, not as a qualitative judgement on the claims made in any particular paper. Our literature search revealed the following papers. The relative amount of studies with presumably global similarity bounds was as follows $(39+13)/(39+13+4) = 0,928$; i.e., > 90%.

Scale-invariant similarity bounds ($r \times$ global SD)

We chose this category, when the article contained the specific information that r was calculated from the original signal (i.e., scale-invariant).

Azami, Fernandez, and Escudero (2017)

Azami, Rostaghi, Abasolo, and Escudero (2017)

Carpentier et al. (2019)

Escudero, Abasolo, Hornero, Espino, and Lopez (2006) [but they note the issue]

Grandy, Garrett, Schmiedek, and Werkle-Bergner (2016)

Hadoush, Alafeef, and Abdulhay (2019)

Kaur et al. (2019)

M. Liu, Song, Liang, Knopfel, and Zhou (2019)

H. Liu et al. (2017) [HRV]

Lu et al. (2015)

McIntosh, Kovacevic, and Itier (2008)

Mizuno et al. (2010)

Weng et al. (2015)

#: 13

Unclear, assumed scale-invariant similarity bounds ($r \times$ global SD)

We chose this category, when the article did not contain any information about how r was calculated, or no reference was made to scale-specific adaptations. For many papers, Costa, Goldberger, and Peng (2002, 2005) or Richman and Moorman (2000) were cited, which use scale-invariant implementations.

Raja Beharelle, Kovacevic, McIntosh, and Levine (2012)

Bertrand et al. (2016)

Catarino, Churches, Baron-Cohen, Andrade, and Ring (2011)

Chen et al. (2015)(HRV)

Chen et al. (2018) (HRV)

Li, Chen, Li, Wang, and Liu (2016)
Chiu et al. (2015) (HRV)
Courtiol et al. (2016)
Gao, Hu, Liu, and Cao (2015)
Harati, Crowell, Huang, Mayberg, and Nemati (2019)
Harati, Crowell, Mayberg, Jun, and Nemati (2016)
Hasegawa et al. (2018)
Heisz and McIntosh (2013)
Heisz, Shedden, and McIntosh (2012)
Hu and Liang (2012) [RM]
Hussain, Saeed, Awan, and Idris (2018)
Hussain, Aziz, et al. (2018)
Jaworska et al. (2018)
Kuntzleman, Jack Rhodes, Harrington, and Miskovic (2018)
Lin et al. (2019) [BOLD]
H. Liu et al. (2018)
H. Y. Liu et al. (2018)
Q. Liu, Chen, Fan, Abbod, and Shieh (2015)
Q. Liu, Chen, Fan, Abbod, and Shieh (2017)
McIntosh et al. (2014)
Misic et al. (2015)
Misic, Vakorin, Paus, and McIntosh (2011)
Miskovic, Owens, Kuntzleman, and Gibb (2016)
Park, Kim, Kim, Cichocki, and Kim (2007)
Roldan, Molina-Pico, Cuesta-Frau, Martinez, and Crespo (2011)
Szostakiwskyj, Willatt, Cortese, and Protzner (2017)
Takahashi et al. (2009)
Takahashi et al. (2010)
Takahashi et al. (2016)
Ueno et al. (2015)
Yang et al. (2013)
H. Y. Wang, McIntosh, Kovacevic, Karachalios, and Protzner (2016)
H. Wang, Pexman, Turner, Cortese, and Protzner (2018)
Wei et al. (2014)

#: 39

Scale-wise similarity bounds (r x scale-wise SD)

We chose this category, when the article either specified that scale-wise recalculation of r parameters was performed, or when the description could allow that inference.

Fabris et al. (2014) [but with unclear variations in r]
Sleimen-Malkoun et al. (2015)
Valencia et al. (2009) [HRV]
Zavala-Yoe, Ramirez-Mendoza, and Cordero (2015)

#: 4

Not applicable

We chose this category, when multi-scale entropy was not used in the study (i.e., erroneous listing of paper).

El-Gohary, McNames, and Elsas (2008)

Erdogan, Yucel, and Akin (2014)
Fernandez, Gomez, Hornero, and Lopez-Ibor (2013)
Heunis, Aldrich, and de Vries (2016)
Hier, Jao, and Brint (1994)
Kielar et al. (2016) [BOLD MSE, single scale]
Nazari et al. (2019)
Puce, Berkovic, Cadusch, and Bladin (1994)
Sinai, Phillips, Chertkow, and Kabani (2010)
Verhaeghe, Gravel, and Reader (2010)
Xu, Cui, Hong, and Liang (2015)

Supplementary References

- Azami, H., Fernandez, A., & Escudero, J. (2017). Refined multiscale fuzzy entropy based on standard deviation for biomedical signal analysis. *Med Biol Eng Comput*, 55(11), 2037-2052. doi:10.1007/s11517-017-1647-5
- Azami, H., Rostaghi, M., Abasolo, D., & Escudero, J. (2017). Refined Composite Multiscale Dispersion Entropy and its Application to Biomedical Signals. *Ieee Transactions on Biomedical Engineering*, 64(12), 2872-2879. doi:10.1109/tbme.2017.2679136
- Bandt, C., & Pompe, B. (2002). Permutation entropy: A natural complexity measure for time series. *Physical Review Letters*, 88(17). doi:10.1103/PhysRevLett.88.174102
- Bertrand, J. A., McIntosh, A. R., Postuma, R. B., Kovacevic, N., Latreille, V., Panisset, M., . . . Gagnon, J. F. (2016). Brain Connectivity Alterations Are Associated with the Development of Dementia in Parkinson's Disease. *Brain Connectivity*, 6(3), 216-224. doi:10.1089/brain.2015.0390
- Carpentier, S. M., McCulloch, A. R., Brown, T. M., Ritter, P., Wang, Z., Salimpoor, V., . . . McIntosh, A. R. (2019). Complexity matching: brain signals mirror environment information patterns during music listening and reward. *bioRxiv*.
- Catarino, A., Churches, O., Baron-Cohen, S., Andrade, A., & Ring, H. (2011). Atypical EEG complexity in autism spectrum conditions: A multiscale entropy analysis. *Clinical Neurophysiology*, 122(12), 2375-2383. doi:10.1016/j.clinph.2011.05.004
- Chen, C. H., Huang, P. W., Tang, S. C., Shieh, J. S., Lai, D. M., Wu, A. Y., & Jeng, J. S. (2015). Complexity of Heart Rate Variability Can Predict Stroke-In-Evolution in Acute Ischemic Stroke Patients. *Sci Rep*, 5, 17552. doi:10.1038/srep17552
- Chen, C. H., Tang, S. C., Lee, D. Y., Shieh, J. S., Lai, D. M., Wu, A. Y., & Jeng, J. S. (2018). Impact of Supratentorial Cerebral Hemorrhage on the Complexity of Heart Rate Variability in Acute Stroke. *Sci Rep*, 8(1), 11473. doi:10.1038/s41598-018-29961-y
- Chiu, H. C., Lin, Y. H., Lo, M. T., Tang, S. C., Wang, T. D., Lu, H. C., . . . Peng, C. K. (2015). Complexity of cardiac signals for predicting changes in alpha-waves after stress in patients undergoing cardiac catheterization. *Scientific Reports*, 5. doi:10.1038/srep13315
- Costa, M., Goldberger, A. L., & Peng, C. K. (2002). Multiscale entropy analysis of complex physiologic time series. *Physical Review Letters*, 89(6). doi:10.1103/PhysRevLett.89.068102
- Costa, M., Goldberger, A. L., & Peng, C. K. (2005). Multiscale entropy analysis of biological signals. *Physical Review E*, 71(2). doi:10.1103/PhysRevE.71.021906
- Courtiol, J., Perdakis, D., Petkoski, S., Muller, V., Huys, R., Sleimen-Malkoun, R., & Jirsa, V. K. (2016). The multiscale entropy: Guidelines for use and interpretation in brain signal analysis. *Journal of Neuroscience Methods*, 273, 175-190. doi:10.1016/j.jneumeth.2016.09.004
- El-Gohary, M., McNames, J., & Elsas, S. (2008). User-guided interictal spike detection. *Conf Proc IEEE Eng Med Biol Soc, 2008*, 821-824. doi:10.1109/iembs.2008.4649280
- Erdogan, S. B., Yucel, M. A., & Akin, A. (2014). Analysis of task-evoked systemic interference in fNIRS measurements: insights from fMRI. *Neuroimage*, 87, 490-504. doi:10.1016/j.neuroimage.2013.10.024
- Escudero, J., Abasolo, D., Hornero, R., Espino, P., & Lopez, M. (2006). Analysis of electroencephalograms in Alzheimer's disease patients with multiscale entropy. *Physiological Measurement*, 27(11), 1091-1106. doi:10.1088/0967-3334/27/11/004

- Fabris, C., Sparacino, G., Sejling, A. S., Goljahani, A., Duun-Henriksen, J., Remvig, L. S., . . . Cobelli, C. (2014). Hypoglycemia-Related Electroencephalogram Changes Assessed by Multiscale Entropy. *Diabetes Technology & Therapeutics*, *16*(10), 688-694. doi:10.1089/dia.2013.0331
- Fernandez, A., Gomez, C., Hornero, R., & Lopez-Ibor, J. J. (2013). Complexity and schizophrenia. *Prog Neuropsychopharmacol Biol Psychiatry*, *45*, 267-276. doi:10.1016/j.pnpbp.2012.03.015
- Gao, J., Hu, J., Liu, F., & Cao, Y. (2015). Multiscale entropy analysis of biological signals: a fundamental bi-scaling law. *Front Comput Neurosci*, *9*, 64. doi:10.3389/fncom.2015.00064
- Grandy, T. H., Garrett, D. D., Schmiedek, F., & Werkle-Bergner, M. (2016). On the estimation of brain signal entropy from sparse neuroimaging data. *Scientific Reports*, *6*. doi:10.1038/srep23073
- Hadoush, H., Alafeef, M., & Abdulhay, E. (2019). Brain Complexity in Children with Mild and Severe Autism Spectrum Disorders: Analysis of Multiscale Entropy in EEG. *Brain Topogr*. doi:10.1007/s10548-019-00711-1
- Harati, S., Crowell, A., Huang, Y., Mayberg, H., & Nemati, S. (2019). Classifying Depression Severity in Recovery from Major Depressive Disorder via Dynamic Facial Features. *IEEE J Biomed Health Inform*. doi:10.1109/jbhi.2019.2930604
- Harati, S., Crowell, A., Mayberg, H., Jun, K., & Nemati, S. (2016). Discriminating clinical phases of recovery from major depressive disorder using the dynamics of facial expression. *Conf Proc IEEE Eng Med Biol Soc, 2016*, 2254-2257. doi:10.1109/embc.2016.7591178
- Hasegawa, C., Takahashi, T., Yoshimura, Y., Nobukawa, S., Ikeda, T., Saito, D. N., . . . Kikuchi, M. (2018). Developmental Trajectory of Infant Brain Signal Variability: A Longitudinal Pilot Study. *Front Neurosci*, *12*, 566. doi:10.3389/fnins.2018.00566
- Heisz, J. J., & McIntosh, A. R. (2013). Applications of EEG Neuroimaging Data: Event-related Potentials, Spectral Power, and Multiscale Entropy. *Jove-Journal of Visualized Experiments*(76). doi:10.3791/50131
- Heisz, J. J., Shedden, J. M., & McIntosh, A. R. (2012). Relating brain signal variability to knowledge representation. *Neuroimage*, *63*(3), 1384-1392. doi:10.1016/j.neuroimage.2012.08.018
- Heunis, T. M., Aldrich, C., & de Vries, P. J. (2016). Recent Advances in Resting-State Electroencephalography Biomarkers for Autism Spectrum Disorder-A Review of Methodological and Clinical Challenges. *Pediatr Neurol*, *61*, 28-37. doi:10.1016/j.pediatrneurol.2016.03.010
- Hier, D. B., Jao, C. S., & Brint, S. U. (1994). The Mental Status Expert (MSE): an expert system for scoring and interpreting the mental status examination. *Proc Annu Symp Comput Appl Med Care*, 1053.
- Hu, M., & Liang, H. (2012). Adaptive multiscale entropy analysis of multivariate neural data. *IEEE Trans Biomed Eng*, *59*(1), 12-15. doi:10.1109/tbme.2011.2162511
- Hussain, L., Aziz, W., Saeed, S., Shah, S. A., Nadeem, M. S. A., Awan, I. A., . . . Kazmi, S. Z. H. (2018). Quantifying the dynamics of electroencephalographic (EEG) signals to distinguish alcoholic and non-alcoholic subjects using an MSE based K-d tree algorithm. *Biomed Tech (Berl)*, *63*(4), 481-490. doi:10.1515/bmt-2017-0041
- Hussain, L., Saeed, S., Awan, I. A., & Idris, A. (2018). Multiscaled Complexity Analysis of EEG Epileptic Seizure Using Entropy-Based Techniques. *Archives of Neuroscience*, *5*(1). doi:10.5812/archneurosci.61161

- Jaworska, N., Wang, H., Smith, D. M., Blier, P., Knott, V., & Protzner, A. B. (2018). Pre-treatment EEG signal variability is associated with treatment success in depression. *Neuroimage Clin*, *17*, 368-377. doi:10.1016/j.nicl.2017.10.035
- Kaur, Y., Ouyang, G., Junge, M., Sommer, W., Liu, M., Zhou, C., & Hildebrandt, A. (2019). The reliability and psychometric structure of Multi-Scale Entropy measured from EEG signals at rest and during face and object recognition tasks. *J Neurosci Methods*, *326*, 108343. doi:10.1016/j.jneumeth.2019.108343
- Kielar, A., Deschamps, T., Chu, R. K., Jokel, R., Khatamian, Y. B., Chen, J. J., & Meltzer, J. A. (2016). Identifying Dysfunctional Cortex: Dissociable Effects of Stroke and Aging on Resting State Dynamics in MEG and fMRI. *Front Aging Neurosci*, *8*, 40. doi:10.3389/fnagi.2016.00040
- Kuntzelman, K., Jack Rhodes, L., Harrington, L. N., & Miskovic, V. (2018). A practical comparison of algorithms for the measurement of multiscale entropy in neural time series data. *Brain Cogn*, *123*, 126-135. doi:10.1016/j.bandc.2018.03.010
- Li, C. X., Chen, Y. N., Li, Y. J., Wang, J., & Liu, T. (2016). Complexity analysis of brain activity in attention-deficit/hyperactivity disorder: A multiscale entropy analysis. *Brain Research Bulletin*, *124*, 12-20. doi:10.1016/j.brainresbull.2016.03.007
- Lin, C., Lee, S. H., Huang, C. M., Chen, G. Y., Ho, P. S., Liu, H. L., . . . Wu, S. C. (2019). Increased brain entropy of resting-state fMRI mediates the relationship between depression severity and mental health-related quality of life in late-life depressed elderly. *J Affect Disord*, *250*, 270-277. doi:10.1016/j.jad.2019.03.012
- Liu, H., Yang, Z., Meng, F., Guan, Y., Ma, Y., Liang, S., . . . Li, L. (2017). Impairment of heart rhythm complexity in patients with drug-resistant epilepsy: An assessment with multiscale entropy analysis. *Epilepsy Research*, *138*, 11-17. doi:10.1016/j.eplepsyres.2017.10.002
- Liu, H., Yang, Z., Meng, F., Huang, L., Qu, W., Hao, H., . . . Li, L. (2018). Chronic vagus nerve stimulation reverses heart rhythm complexity in patients with drug-resistant epilepsy: An assessment with multiscale entropy analysis. *Epilepsy Behav*, *83*, 168-174. doi:10.1016/j.yebeh.2018.03.035
- Liu, H. Y., Yang, Z., Meng, F. G., Guan, Y. G., Ma, Y. S., Liang, S. L., . . . Li, L. M. (2018). Preoperative Heart Rate Variability as Predictors of Vagus Nerve Stimulation Outcome in Patients with Drug-resistant Epilepsy. *Sci Rep*, *8*(1), 3856. doi:10.1038/s41598-018-21669-3
- Liu, M., Song, C., Liang, Y., Knopfel, T., & Zhou, C. (2019). Assessing spatiotemporal variability of brain spontaneous activity by multiscale entropy and functional connectivity. *Neuroimage*, *198*, 198-220. doi:10.1016/j.neuroimage.2019.05.022
- Liu, Q., Chen, Y. F., Fan, S. Z., Abbod, M. F., & Shieh, J. S. (2015). EEG Signals Analysis Using Multiscale Entropy for Depth of Anesthesia Monitoring during Surgery through Artificial Neural Networks. *Computational and Mathematical Methods in Medicine*. doi:10.1155/2015/232381
- Liu, Q., Chen, Y. F., Fan, S. Z., Abbod, M. F., & Shieh, J. S. (2017). EEG artifacts reduction by multivariate empirical mode decomposition and multiscale entropy for monitoring depth of anaesthesia during surgery. *Medical & Biological Engineering & Computing*, *55*(8), 1435-1450. doi:10.1007/s11517-016-1598-2
- Lu, W. Y., Chen, J. Y., Chang, C. F., Weng, W. C., Lee, W. T., & Shieh, J. S. (2015). Multiscale Entropy of Electroencephalogram as a Potential Predictor for the Prognosis of Neonatal Seizures. *Plos One*, *10*(12). doi:10.1371/journal.pone.0144732

- McIntosh, A. R., Kovacevic, N., & Itier, R. J. (2008). Increased Brain Signal Variability Accompanies Lower Behavioral Variability in Development. *Plos Computational Biology*, 4(7). doi:10.1371/journal.pcbi.1000106
- McIntosh, A. R., Vakorin, V., Kovacevic, N., Wang, H., Diaconescu, A., & Protzner, A. B. (2014). Spatiotemporal Dependency of Age-Related Changes in Brain Signal Variability. *Cerebral Cortex*, 24(7), 1806-1817. doi:10.1093/cercor/bht030
- Misic, B., Doesburg, S. M., Fatima, Z., Vidal, J., Vakorin, V. A., Taylor, M. J., & McIntosh, A. R. (2015). Coordinated Information Generation and Mental Flexibility: Large-Scale Network Disruption in Children with Autism. *Cerebral Cortex*, 25(9), 2815-2827. doi:10.1093/cercor/bhu082
- Misic, B., Vakorin, V. A., Paus, T., & McIntosh, A. R. (2011). Functional embedding predicts the variability of neural activity. *Frontiers in Systems Neuroscience*, 5, 90. doi:10.3389/fnsys.2011.00090
- Miskovic, V., Owens, M., Kuntzelman, K., & Gibb, B. E. (2016). Charting moment-to-moment brain signal variability from early to late childhood. *Cortex*, 83, 51-61. doi:10.1016/j.cortex.2016.07.006
- Mizuno, T., Takahashi, T., Cho, R. Y., Kikuchi, M., Murata, T., Takahashi, K., & Wada, Y. (2010). Assessment of EEG dynamical complexity in Alzheimer's disease using multiscale entropy. *Clinical Neurophysiology*, 121(9), 1438-1446. doi:10.1016/j.clinph.2010.03.025
- Nazari, A., Alavimajd, H., Shakeri, N., Bakhshandeh, M., Faghihzadeh, E., & Marzbani, H. (2019). Prediction of Brain Connectivity Map in Resting-State fMRI Data Using Shrinkage Estimator. *Basic Clin Neurosci*, 10(2), 147-156. doi:10.32598/bcn.9.10.140
- Ouyang, G. X., Li, J., Liu, X. Z., & Li, X. L. (2013). Dynamic characteristics of absence EEG recordings with multiscale permutation entropy analysis. *Epilepsy Research*, 104(3), 246-252. doi:10.1016/j.eplepsyres.2012.11.003
- Park, J. H., Kim, S., Kim, C. H., Cichocki, A., & Kim, K. (2007). Multiscale entropy analysis of EEG from patients under different pathological conditions. *Fractals-Complex Geometry Patterns and Scaling in Nature and Society*, 15(4), 399-404. doi:10.1142/S0218348x07003691
- Puce, A., Berkovic, S. F., Cadusch, P. J., & Bladin, P. F. (1994). P3 latency jitter assessed using 2 techniques. I. Simulated data and surface recordings in normal subjects. *Electroencephalogr Clin Neurophysiol*, 92(4), 352-364. doi:10.1016/0168-5597(94)90103-1
- Raja Beharelle, A., Kovacevic, N., McIntosh, A. R., & Levine, B. (2012). Brain signal variability relates to stability of behavior after recovery from diffuse brain injury. *Neuroimage*, 60(2), 1528-1537. doi:10.1016/j.neuroimage.2012.01.037
- Richman, J. S., & Moorman, J. R. (2000). Physiological time-series analysis using approximate entropy and sample entropy. *American Journal of Physiology-Heart and Circulatory Physiology*, 278(6), H2039-H2049.
- Riedl, M., Muller, A., & Wessel, N. (2013). Practical considerations of permutation entropy. *European Physical Journal-Special Topics*, 222(2), 249-262. doi:10.1140/epjst/e2013-01862-7
- Roldan, E. M., Molina-Pico, A., Cuesta-Frau, D., Martinez, P. M., & Crespo, S. O. (2011). Characterization of entropy measures against data loss: application to EEG records. *Conf Proc IEEE Eng Med Biol Soc*, 2011, 6110-6113. doi:10.1109/iembs.2011.6091509

- Sinai, M., Phillips, N. A., Chertkow, H., & Kabani, N. J. (2010). Task switching performance reveals heterogeneity amongst patients with mild cognitive impairment. *Neuropsychology*, 24(6), 757-774. doi:10.1037/a0020314
- Sleimen-Malkoun, R., Perdakis, D., Muller, V., Blanc, J. L., Huys, R., Temprado, J. J., & Jirsa, V. K. (2015). Brain Dynamics of Aging: Multiscale Variability of EEG Signals at Rest and during an Auditory Oddball Task(1,2,3). *Eneuro*, 2(3). doi:10.1523/ENEURO.0067-14.2015
- Szostakiwskyj, J. M. H., Willatt, S. E., Cortese, F., & Protzner, A. B. (2017). The modulation of EEG variability between internally-and externally-driven cognitive states varies with maturation and task performance. *Plos One*, 12(7). doi:10.1371/journal.pone.0181894
- Takahashi, T., Cho, R., Mizuno, T., Kikuchi, M., Murata, T., Takahashi, K., & Wada, Y. (2010). Antipsychotics reverse abnormal EEG complexity in drug-naive schizophrenia: A multiscale entropy analysis. *International Journal of Neuropsychopharmacology*, 13, 242-243.
- Takahashi, T., Cho, R. Y., Murata, T., Mizuno, T., Kikuchi, M., Mizukami, K., . . . Wada, Y. (2009). Age-related variation in EEG complexity to photic stimulation: A multiscale entropy analysis. *Clinical Neurophysiology*, 120(3), 476-483. doi:10.1016/j.clinph.2008.12.043
- Takahashi, T., Yoshimura, Y., Hiraishi, H., Hasegawa, C., Munesue, T., Higashida, H., . . . Kikuchi, M. (2016). Enhanced brain signal variability in children with autism spectrum disorder during early childhood. *Human Brain Mapping*, 37(3), 1038-1050. doi:10.1002/hbm.23089
- Ueno, K., Takahashi, T., Takahashi, K., Mizukami, K., Tanaka, Y., & Wada, Y. (2015). Neurophysiological basis of creativity in healthy elderly people: A multiscale entropy approach. *Clinical Neurophysiology*, 126(3), 524-531. doi:10.1016/j.clinph.2014.06.032
- Valencia, J. F., Porta, A., Vallverdu, M., Claria, F., Baranowski, R., Orłowska-Baranowska, E., & Caminal, P. (2009). Refined Multiscale Entropy: Application to 24-h Holter Recordings of Heart Period Variability in Healthy and Aortic Stenosis Subjects. *Ieee Transactions on Biomedical Engineering*, 56(9), 2202-2213. doi:10.1109/Tbme.2009.2021986
- Verhaeghe, J., Gravel, P., & Reader, A. J. (2010). Task-oriented quantitative image reconstruction in emission tomography for single- and multi-subject studies. *Phys Med Biol*, 55(23), 7263-7285. doi:10.1088/0031-9155/55/23/006
- Wang, H., Pexman, P. M., Turner, G., Cortese, F., & Protzner, A. B. (2018). The relation between Scrabble expertise and brain aging as measured with EEG brain signal variability. *Neurobiology of Aging*, 69, 249-260. doi:10.1016/j.neurobiolaging.2018.05.015
- Wang, H. Y., McIntosh, A. R., Kovacevic, N., Karachalios, M., & Protzner, A. B. (2016). Age-related Multiscale Changes in Brain Signal Variability in Pre-task versus Post-task Resting-state EEG. *Journal of Cognitive Neuroscience*, 28(7), 971-984. doi:10.1162/jocn_a_00947
- Wei, Q., Li, Y., Fan, S. Z., Liu, Q., Abbod, M. F., Lu, C. W., . . . Shieh, J. S. (2014). A critical care monitoring system for depth of anaesthesia analysis based on entropy analysis and physiological information database. *Australasian Physical & Engineering Sciences in Medicine*, 37(3), 591-605. doi:10.1007/s13246-014-0285-6

- Weng, W. C., Jiang, G. J., Chang, C. F., Lu, W. Y., Lin, C. Y., Lee, W. T., & Shieh, J. S. (2015). Complexity of Multi-Channel Electroencephalogram Signal Analysis in Childhood Absence Epilepsy. *Plos One*, *10*(8), e0134083. doi:10.1371/journal.pone.0134083
- Xu, Y., Cui, J., Hong, W., & Liang, H. (2015). [Automatic Classification of Epileptic Electroencephalogram Signal Based on Improved Multivariate Multiscale Entropy]. *Sheng Wu Yi Xue Gong Cheng Xue Za Zhi*, *32*(2), 256-262.
- Yang, A. C., Wang, S. J., Lai, K. L., Tsai, C. F., Yang, C. H., Hwang, J. P., . . . Fuh, J. L. (2013). Cognitive and neuropsychiatric correlates of EEG dynamic complexity in patients with Alzheimer's disease. *Progress in Neuro-Psychopharmacology & Biological Psychiatry*, *47*, 52-61. doi:10.1016/j.pnpbp.2013.07.022
- Zanin, M., Zunino, L., Rosso, O. A., & Papo, D. (2012). Permutation Entropy and Its Main Biomedical and Econophysics Applications: A Review. *Entropy*, *14*(8), 1553-1577. doi:10.3390/e14081553
- Zavala-Yoe, R., Ramirez-Mendoza, R., & Cordero, L. M. (2015). Novel way to investigate evolution of children refractory epilepsy by complexity metrics in massive information. *Springerplus*, *4*. doi:10.1186/s40064-015-1173-6